Title
HYPERFINE-STRUCTURE STUDIES OF Er169 AND ISOTOPES OF REFRACTORY ELEMENTS

Author
Doyle, Walter M.

Publication Date
1963-01-23

UCRL-10609

University of California

Ernest O. Lawrence Radiation Laboratory

HYPERFINE-STRUCTURE STUDIES OF Er^{169} AND ISOTOPES OF REFRACTORY ELEMENTS

DISCLAIMER

Research and Development

UCRL-10609
UC-34 Physics
(TID-4500, 18th Edition)

UNIVERSITY OF CALIFORNIA

Lawrence Radiation Laboratory
Berkeley, California

Contract No. W-7405-eng-48

HYPERFINE-STRUCTURE STUDIES OF Er^{169} AND ISOTOPES OF REFRACTORY ELEMENTS

Walter M. Doyle
(Ph. D. Thesis)

January 23, 1963

Printed in USA. Price $2.00. Available from the
Office of Technical Services
U. S. Department of Commerce
Washington 25, D.C.

HYPERFINE-STRUCTURE STUDIES OF Er^{169} AND ISOTOPES OF REFRACTORY ELEMENTS

Contents

HYPERFINE-STRUCTURE STUDIES OF Er^{169} AND ISOTOPES OF REFRACTORY ELEMENTS

Walter M. Doyle

Lawrence Radiation Laboratory
University of California
Berkeley, California

January 23, 1963

ABSTRACT

The atomic-beam magnetic-resonance method has been used to investigate the electronic and nuclear properties of Er^{169} and to determine the spins of several refractory-group nuclides.

The apparatus used in the erbium research was sufficiently accurate to allow measurement of the nuclear dipole moment directly through its interaction with the external magnetic field. Investigations carried out in the $^3H_6$ electronic ground state yielded the results

$$A = 725.46(31) \text{ Mc},$$

$$g_I = 5.55(27) \times 10^{-4},$$

and

$$g_J = -1.16381(5),$$

where A is the dipole interaction constant, g_I and g_J are the nuclear and electronic g factors, respectively, expressed in terms of the Bohr megneton, and the nuclear spin $I = 1/2$ had previously been determined. The value of the nuclear moment

$$\mu_I = +0.513(25) \text{ nm}$$

derived from g_I and corrected for diamagnetic shielding is consistent with the value inferred from the interaction constant if the $\langle 1/r^3 \rangle$

value of Lindgren is used and the possible effects of configuration mixing are neglected.

Beams of refractory metals were produced by electron bombardment of narrow wire sources, and the spins of several nuclides were measured. These are listed below along with the half-lives and the electronic states in which resonances were observed.

Isotope	Half-life	Nuclear spin	Observed states
Tantalum-183	5 days	7/2	$[(5d)^3 - {}^4F_{5/2,\,7/2}]$
Tungsten-185	74 days	3/2	$[(5d)^4 - {}^5D_{1,2,3}][(5d)^5(6s) - {}^7S_3]$
Tungsten-187	24 hours	3/2	$[(5d)^4 - {}^5D_{1,2,3}][(5d)^5(6s) - {}^7S_3]$
Rhenium-186	91 hours	1	$[(5d)^5 - {}^6S_{5/2}]$
Rhenium-188	17 hours	1	$[(5d)^5 - {}^6S_{5/2}]$
Iridium-192	74 days	4	$[(5d)^7 - {}^4F_{9/2}][(5d)^8(6s) - {}^4F_{9/2}]$
Iridium-194	19 hours	1	$[(5d)^7 - {}^4F_{9/2}][(5d)^8(6s) - {}^4F_{9/2}]$

The experiments are discussed and the results interpreted in the light of current atomic and nuclear theory.

I. INTRODUCTION

The subject of this paper is a series of hyperfine-structure investigations of free atoms performed by using the atomic-beam magnetic-resonance flop-in technique. The work covered consists of two independent projects, the aims and consequences of which are treated in detail in later sections.

The direct measurements of the nuclear magnetic-dipole moment of Er^{169} was attempted in a effort to obtain information about the electronic matrix elements entering into the calculation of rare earth nuclear moments from hyperfine-structure data. The successful completion of the experiment necessitated the use of atomic-beam apparatus of high resolution. The magnetic field in the transition region of the apparatus used was sufficiently uniform to allow determination of resonant frequencies to within a few parts in 10^6.

The second project discussed resulted in the determination of the nuclear spins of a number of radioactive isotopes of refractory elements. Application of atomic-beam techniques in this region was made possible by the development of a suitable method of beam production. The nuclear properties of the refractories are of considerable interest because the region is characterized by a gradual transition from highly deformed to nearly spherical nuclei. Our results serve as a test of the applicability of the strong-deformation model.

Section II is concerned with those aspects of the research common to both projects, whereas the individual aspects is treated in Secs. III and IV. The treatment is confined to that material necessary for an understanding of the purpose, techniques, and results of the research. Although reference is made to particular background material during the course of the dissertation, I recommend as a general reference the review article "On Atomic Beams" by R. Marrus and W. A. Nierenberg.[1]

II. GENERAL THEORY, METHODS, AND APPARATUS

A. Hyperfine Structure of a Free Atom

The noncentral or hyperfine-structure interaction between a nucleus and the surrounding electronic system has been treated thoroughly in the literature.[2,3,4] It suffices at this time to simply state those results relevant to the present work.

The largest contributions to the hfs Hamiltonian come from the magnetic-dipole and electric-quadrupole interactions. Neglecting higher-order effects, one has

$$\mathcal{H}_{hfs} = (-\overline{\mu}_n \cdot \overline{H}_e) - e^2 \sum_{i,n} \frac{r_n^2}{r_i^3} \sum_k (-1)\, C_k^{(2)}(\theta_n,\phi_n)\, C_{-k}^{(2)}(\theta_i,\phi_i)\,, \tag{1}$$

where $\overline{\mu}_n$ is the nuclear magnetic dipole-moment operator, $\overline{H}_e$ is the operator corresponding to the magnetic field of the electrons at the nucleus, e is the electronic charge, r_i and r_n are the electronic and nuclear radial coordinates, respectively, and $C_k^{(2)}$ is related to a spherical harmonic. The first summation is taken over electrons (i) and protons (n).

Hyperfine-structure energies are normally very small compared with separations between electronic or nuclear-energy levels. As a result, the magnitudes of the total electronic and nuclear angular momenta $\overline{J}$ and $\overline{I}$, respectively, are to a good approximation conserved, and only the first-order contribution to the hfs energy need be calculated. A complete determination of a state of the coupled system requires specification of a set of four quantum numbers. In addition to I and J, it is convenient to use eigenvalues of the magnitude of the total angular momentum $\overline{F} = \overline{I} + \overline{J}$ and its z component F_z, both of which commute with $\mathcal{H}_{hfs}$. In this representation

$$W_{hfs}(F,m_F) = \left\langle IJFm_F \middle| \mathcal{H}_{hfs} \middle| IJFm_F \right\rangle = \frac{aK}{2} + b\, \frac{\frac{3}{8}[K(K+1) - \left\{\frac{4}{3}\right| I(I+1)J(J+1)]}{I(2I-1)J(2J-1)}\,, \tag{2}$$

where

$$K = F(F+1) - I(I+1) - J(J+1) ,$$

$$a = -\frac{1}{IJ}\,\mu_I \left\langle H_{e,z} \right\rangle_{J,(m_j = J)},$$

and

$$b = e^2 q_j Q ,$$

with

$$\left\langle H_{e,z} \right\rangle_{J,J} = -2\mu_0 \sum_i \left\langle \frac{1}{r^3} \right\rangle_i \left\langle J,J \left| \left\{ l_z - s_z + \frac{3z(\bar{s}\cdot\bar{r})}{r^2} \right\}_i \right| J,J \right\rangle \tag{3}$$

and

$$q_J = \sum_i \left\langle \frac{1}{r^3} \right\rangle_i \left\langle J,J \left| (3\cos^2\theta_i - 1) \right| J,J \right\rangle . \tag{4}$$

Here, q_J is the electric field-gradient parameter, and the nuclear electric-quadrupole moment is defined by

$$Q = \left\langle I,\ (m_I = I) \left| \sum_n r_n{}^2 (3\cos^2\theta_n - 1) \right| I,\ (m_I = I) \right\rangle . \tag{5}$$

The quantity μ_I, generally referred to as the nuclear-dipole moment, is the maximum observable component of the vector dipole-moment operator,

$$\mu_I = \left\langle I,\ (m_I = I) \left| \mu_{n,z} \right| I,\ (m_I = I) \right\rangle . \tag{6}$$

The effect of an external magnetic field is described by two additional terms in the Hamiltonian,

$$\begin{aligned} \mathcal{H}_{ext} &= -\bar{\mu}_e \cdot \bar{H}_0 - \bar{\mu}_n \cdot \bar{H}_0 \\ &= -g_J \mu_0 \bar{J} \cdot \bar{H}_0 - g_I \mu_0 \bar{I} \cdot \bar{H}_0 , \end{aligned} \tag{7}$$

where I^2 and J^2 are still assumed to be conserved, and g_J and g_I (the electronic and nuclear g factors) are defined by

$$g_J = \frac{1}{\mu_0} \frac{\langle J,J|\mu_{e,z}|J,J\rangle}{\langle J,J|J_z|J,J\rangle} = \frac{1}{\mu_0}\left(\frac{\mu_J}{J}\right),$$

and (8)

$$g_I = \frac{1}{\mu_0} \frac{\langle I,I|\mu_{n,z}|I,I\rangle}{\langle I,I|I_z|I,I\rangle} = \frac{1}{\mu_0}\left(\frac{\mu_I}{I}\right) .$$

If $\mathcal{H}_{ext}$ is small compared with $\mathcal{H}_{hfs}$, it may be treated as a perturbation

$$W^1_{ext}(F, m_F) = -g_F \mu_0 m_F H_0 , \tag{9}$$

where

$$g_F = g_J \frac{F(F+1)+J(J+1)-I(I+1)}{2F(F+1)} + g_I \frac{F(F+1)+I(I+1)-J(J+1)}{2F(F+1)} .$$

If, on the other hand, the interaction with the external field is dominant, then the isotropy of space is destroyed, and the magnitude at the total angular momentum is not conserved. It is then convenient to use the representation $|I, J, m_I, m_J\rangle$, since $\mathcal{H}_{ext}$ commutes with I_z and J_z. In this case, $\mathcal{H}_{hfs}$ may be treated by perturbation theory:

$$W_{ext}(m_I, m_J) = -g_J \mu_0 m_J H_0 - g_I \mu_0 m_I H_0 \qquad (10)$$

and

$$W^1_{hfs}(m_I, m_J) = am_I m_J + b \frac{[3m_J^2 - J(J+1)][3m_I^2 - I(I+1)]}{4J(2J-1)I(2I-1)} \qquad (11)$$

An exact determination of the energy eigenvalues of the total Hamiltonian would involve diagonalization of a $(2I+1)(2J+1)$-order energy matrix that would factor into submatrices corresponding to the values of the rigorous quantum number m_f.

B. The Atomic-Beam Magnetic-Resonance Method

Atomic-beam techniques may be used to facilitate observation of transitions between energy levels of the Hamiltonian $\mathcal{H} = \mathcal{H}_{hfs} + \mathcal{H}_{ext}$ and hence to obtain information about the parameters I, J, g_I, g_J, a, and b. The magnetic-resonance method as applied here is based on the early work of Rabi and Zacharias.[5, 6, 7]

The machine geometry is shown schematically in Fig. 1. The basic features are two strongly inhomogeneous magnets A and B, which act as polarizer and analyzer, respectively, and a transition region consisting of a radio-frequency field superimposed on a uniform magnetic field C. In the A and B regions the predominant contribution to the energy arises from the term $-g_J \mu_0 m_J H_0$, and an atom is subject to a deflecting force $F \approx +g_J \mu_0 m_J \partial H_0/\partial z$. The fields are normally adjusted so that only those atoms undergoing transitions in the C region that lead to a reversal of the sign of m_J will be refocused.

Atoms emerging from the source 0 enter the A magnet gap where they undergo deflection. Those having suitable combinations of source angle, magnetic quantum number, and velocity pass through the collimator into the C region. If the proper transition takes place, the direction of the deflecting force is reversed in the B magnet, and atoms follow path 2 to the detector D. If the condition $m_J \rightarrow -m_J$ is not fulfilled, the atoms are deflected into the pole tipe (path 1). The stop wire

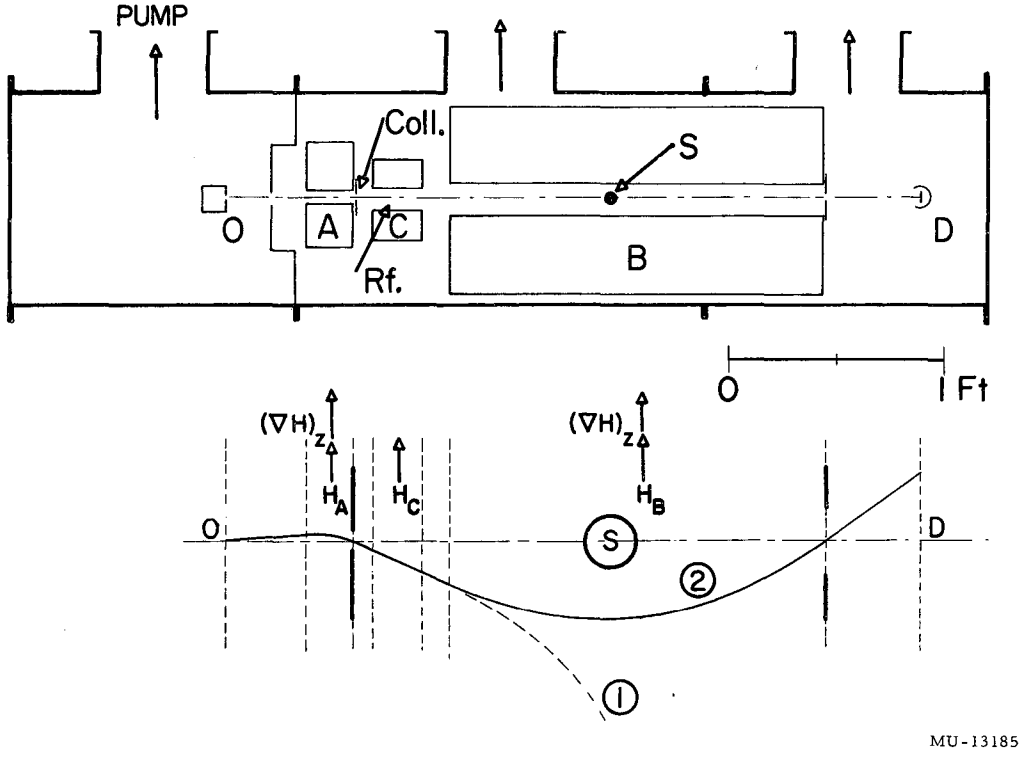

Fig. 1. Atomic beam machine geometry with typical beam paths (schematic).

S prevents fast atoms and those having $m_J = 0$ from reaching the detector.

Transitions in the C region are subject to the usual selection rules for magnetic dipole radiation.[8] In the weak-field case ($\mathcal{H}_{ext} \ll \mathcal{H}_{hfs}$),

$$\Delta m_F = 0 \text{ with } \Delta F = \pm 1 ,$$

or (12)

$$\Delta m_F = \pm 1 \text{ with } \Delta F = \pm 1, 0 .$$

The $\Delta m_F = 0$ transitions are possible only if there is a component of the oscillating magnetic field parallel to the uniform C field. For strong fields,

$$\Delta m_J = 0 \text{ with } \Delta m_I = \pm 1 ,$$

or (13)

$$\Delta m_I = 0 \text{ with } \Delta m_J = \pm 1 .$$

In addition to the allowed transitions listed above, multiple quantum transitions for which Δm is greater than one are often observed.

C. Apparatus and Operating Procedure

The two atomic-beam machines used in this research have been fully described previously. Machine A (Fig. 2) discussed by Brink, among others, is of "conventional" construction, with most of the components inside the vacuum system.[9, 10, 11] Machine B (Fig. 3) is of the "inside-out" variety, having the magnet coils exposed. It has recently been rebuilt by White, and yields extremely narrow resonances.[12] For erbium, the full width at half maximum is of the order of 30 kc/sec at the highest fields used ($\approx$ 800 G), while machine A exhibited a full width at the same fields of about 600 kc/sec. Since

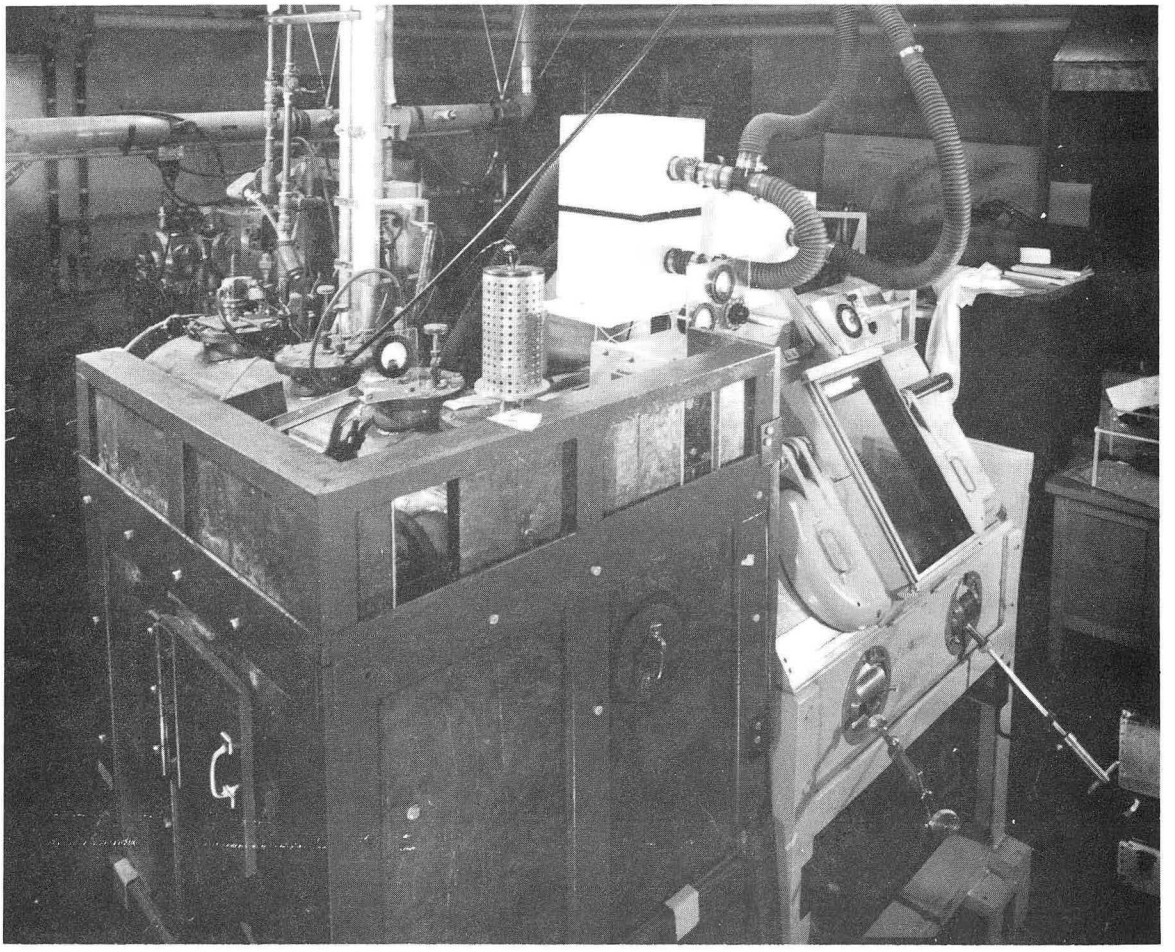

ZN-2590

Fig. 2. Atomic beam machine A.

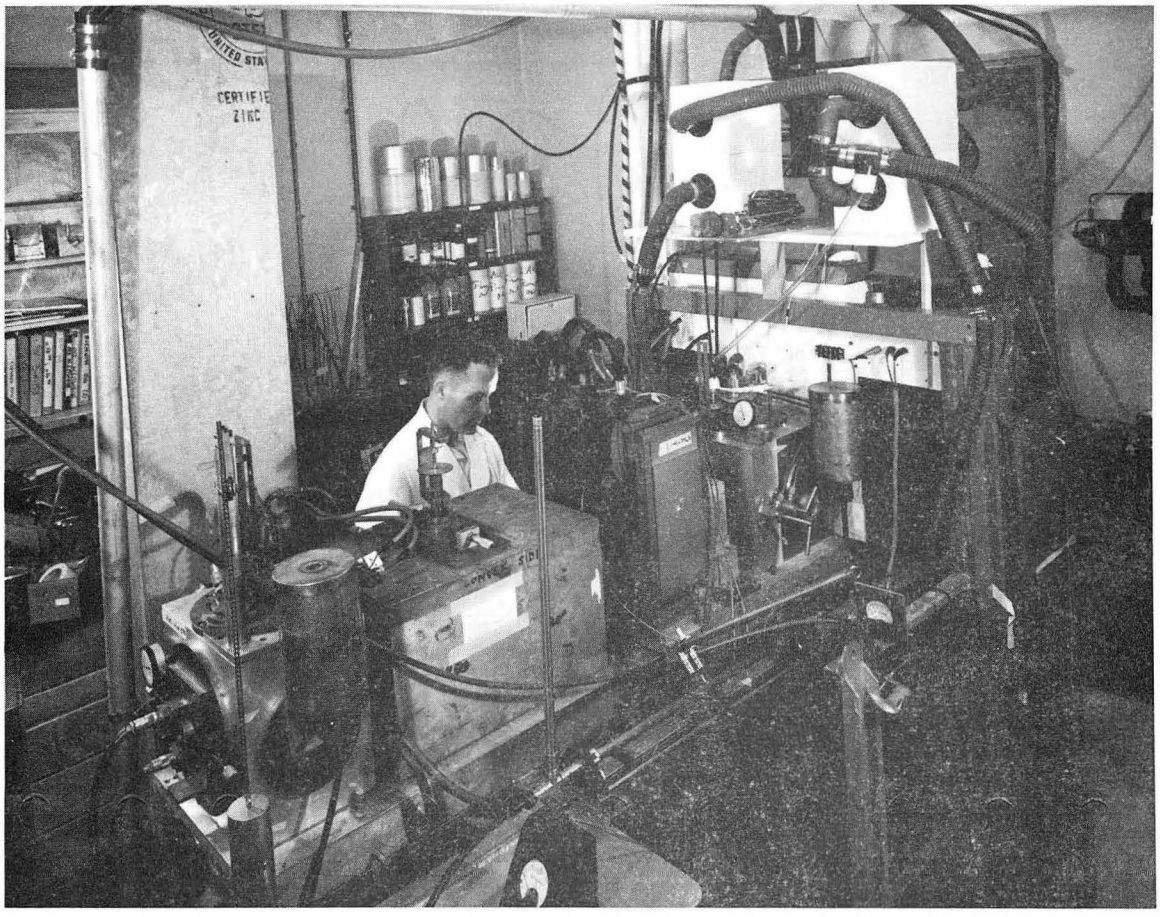

ZN-3401

Fig. 3. Atomic beam machine B.

machine A generally yields a greater resonance height, it was used for the refractory work, where precision was a minor consideration, and for the earlier erbium runs.

The isotopes studies were produced by thermal-neutron bombardment of the natural metals. The operations of capsule opening and loading of the sample into the machine were carried out in shielded glove boxes. Beam-production methods differed for the two projects and are discussed later.

The radioactive atomic beams were in each case detected by collection on flamed platinum foils and subsequent β counting in continuous-flow methane counters. Decay plots of individual foils served to identify the isotopes present.

The magnetic C field was calibrated by monitoring the observable $\Delta F = 0$, $\Delta m_F = \pm 1$ transition in K^{39}. For this purpose, an oven containing potassium is positioned in front of the regular source. When not in use, it may be lifted out of the path of the radioactive beam. Potassium has a low enough ionization potential so that an appreciable percentage of the atoms are ionized on striking a hot tungsten strip. Introduction of a negative electrode and measurement of the resulting ion current then provide a convenient direct method of detection.

The general operating procedure was to alternate, 5-min exposures at specific field and frequency settings with 1-min "direct-beam" exposures (i.e., with the stop wire removed from the beam path). The average of two direct-beam exposures is then used for normalization. The high resolution of machine B necessitated recalibration of the C field after every 5-min exposure. Noticeable drift was rarely observed with machine A, and the field was usually monitored after four or five exposures.

III. HYPERFINE STRUCTURE OF ERBIUM-169

A. Introduction

About thirty-five nuclear moments in the rare earth region have been determined from paramagnetic-resonance and atomic-beam data. At the time our investigations were undertaken, little direct information about the moments was available, and it had been necessary in most cases to infer their values from the measured interaction constants by means of theoretical calculations involving considerable uncertainty. Much of this uncertainty arose from the sensitivity of $\left\langle \frac{1}{r^3} \right\rangle$ to the form of the electronic wave function. The project of measuring, by atomic-beam magnetic resonance, the interaction constant A and the magnetic moment μ_I of Er^{169} was therefore undertaken in order to obtain information about the values of $\left\langle \frac{1}{r^3} \right\rangle$ for the rare earths.

The method of nuclear magnetic resonance -- commonly used to measure nuclear moments directly -- has not been used successfully in most of the rare-earth region owing to the paramagnetism of the nonvalent 4f electrons. Difficulty also arises in applying the atomic-beam method to the problem, since the nuclear moment contributes a relatively small term to the Hamiltonian characterizing the interaction with an external field:

$$\mathcal{H}_{ext} = -g_J \mu_0 \overline{J} \cdot \overline{H}_0 - g_I \mu_0 \overline{I} \cdot \overline{H}_0 .$$

Not only are nuclear g factors of the order of $\frac{1}{2000}$ times the electronic ones, but for Er^{169}, J equals 12 I, so that the effect of the nuclear term on the Hamiltonian is about 5 parts in 10^5. To determine transition frequencies with sufficient accuracy to measure g_I, it is necessary to obtain very stable atomic beams and high resonance intensity. Erbium has proved very satisfactory in these respects. The high intensity is at least in part a result of the relatively small total number of substates. The beam strength was observed to be relatively constant, varying less than 10% for operating periods of more than 1h.

Earlier atomic-beam investigations in this Laboratory yielded the nuclear-spin ($I = 1, 2$) and ground-state electronic angular momentum ($J = 6$).[13] No other electronic states were observed. The hyperfine structure of such a system is shown schematically in Fig. 4.

A system with angular momentum $1/2$ cannot experience a quadrupole interaction. It is seen, for example, that the projection factors for the quadrupole interaction in Eq. (2) and in Eq. (11) vanish for $I = 1/2$. In addition, the observable quadrupole moment Q can be shown to vanish.[3] Thus, in the approximation that I^2 and J^2 are conserved, the Hamiltonian $\mathcal{H} = \mathcal{H}_{hfs} + \mathcal{H}_{ext}$ may be written

$$\mathcal{H} = a\,\overline{I}\cdot\overline{J} - g_J\mu_0\,\overline{J}\cdot\overline{H}_0 - g_I\mu_0\,\overline{I}\cdot\overline{H}_0 . \tag{14}$$

We can gain an idea of the dependence of the two observable transitions (Fig. 4) on the nuclear moment by studying their behavior in the low- and high-field limits. In the low-field (or Zeeman) region, we obtain from Eq. (9)

$$\nu = -g_F \frac{\mu_0 H}{h} ,$$

with (15)

$$g_F = g_J \frac{F(F+1)+J(J+1)-I(I+1)}{2F(F+1)} + g_I \frac{F(F+1)+I(I+1)-J(J+1)}{2F(F+1)} ,$$

and in the Pachen-Bach region (Eqs. 10 and 11), we obtain

$$\nu = -g_J \frac{\mu_0 H}{h} \pm \frac{a}{2} , \tag{16}$$

where the upper sign holds for the α transition ($F = \frac{13}{2}$) and the lower sign holds for the β transition. It should be apparent that a large hyperfine-structure separation aF_{max} is advantageous in this

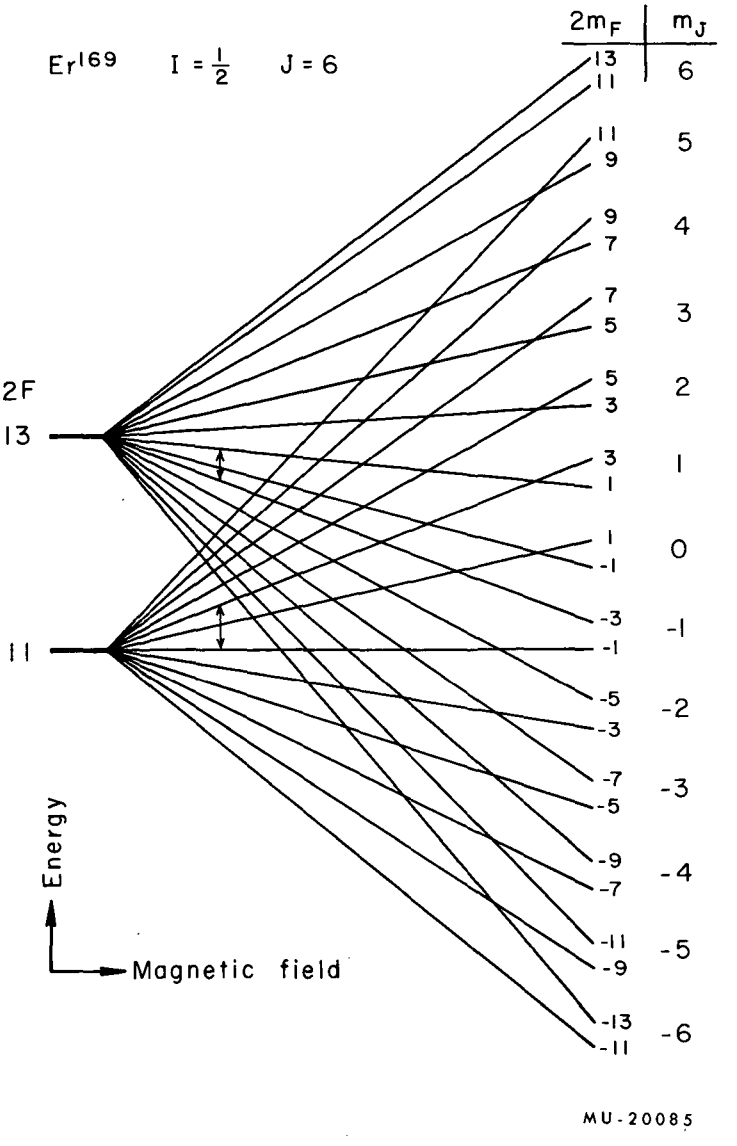

Fig. 4. Hfs levels of Er^{169} (schematic).

work, since the resolution of our apparatus increases with magnetic field while the dependence of the transition frequencies on g_I vanishes as $\overline{\mu}_e \cdot \overline{H}_0$ becomes large compared with aF_{max}. One might expect a relatively large hyperfine separation for Er^{169}, since $F_{max} = \frac{13}{2}$.

B. Experimental Methods and Results

The radioactive isotope Er^{169} ($T_{1/2} = 9.4$ days) was produced by thermal neutron bombardment of natural erbium metal in the General Electric test reactor at Vallecitos. Bombardment of 500 mg of the metal for 5 days at 9×10^{13} neutrons $/cm^2/sec$ yields about 0.7 Ci of Er^{169}, enough to last 10 to 12 h under normal operating conditions. In practice, each sample was allowed to decay at least 2 days before being used to insure predominance of the 9.4-day isotope over the 7-h Er^{171}. The beam was produced by electron bombardment of a tantalum oven containing the erbium sample. The oven and filament were mounted in an oven loader that could be removed without destroying the machine vacuum.[10, 12]

The hyperfine structure was investigated by studying the field dependence of the two observable transitions. Resonances were first traced out in the low-field region where their frequencies are reliably predicted by Eq. (15). They were then followed to higher fields by using, firstly, linear extrapolation and, later, quadratic extrapolation. When appreciable deviation from linearity had been observed, attempts were made to fit values of the parameters a, g_I, and g_J to the field-vs-frequency data by using an IBM 709 computer routine that diagonalizes the approximate Hamiltonian (Eq. 14) in the F, m_F representation and performs a least-squares fit.[1, 14]

The experiment was performed in two steps. Firstly, by using machine A, observations were made at fields up to about 800 G. The data obtained were sufficient to yield a value of "a" with an uncertainty of a few percent but gave no direct information about g_I. Most of the high-field resonances were then retraced by using machine B. The new data exhibited a somewhat reduced resonance intensity but also much better resolution owing to the greater uniformity

of the C field. In fact, the resonance width was observed to diminish with increasing field; thus indicated a spreading of the rf signal through more of the C region. Field inhomogeneity in machine A had caused the width of the original curves to increase with the field. Sample resonances are shown in Figs. 5 and 6.

The best fit to our data was obtained with $A = 725.46(31)$ Mc, $g_J = -1.163810(1)$, and $g_I = 5.55(27) \times 10^{-4}$, where the errors quoted represent two standard deviations. Frequencies calculated by using these parameters are compared with the observed frequencies in Table I. The nuclear magnetic moment is obtained from g_I by using the relation $\mu_I = \mu_0 I g_I$ (corrected), Eq. (8), where g_I has been multiplied by the factor $\gamma = 1.0078$ to correct for diamagnetic shielding by the electrons.[15] The result is $\mu_I = 0.513(25)$ nm.

C. Discussion of Possible Errors

The most obvious of the possible sources of error in our work are uncertainties in oscillator frequency and field setting. We feel that, by using a transfer oscillator and frequency counter, we were able to hold the frequency to within 1 kc of a desired value averaged over a 5-min exposure. In addition, we were able to adjust the field to within about $\frac{1}{20}$ of the K^{39} line width. The setting was checked after each exposure so that if any drift had occurred the exposure could be repeated. Since the errors involved would most likely be random, our ability to maintain frequency and field settings is reflected in our success in fitting a Lorentian curve to a series of 8 to 14 consecutive points.

During the course of the experiment it was found that the fringing field of the nearby Bevatron caused frequency shifts of about 10 kc. This occurred because the radioactive method of detection used with erbium yielded essentially a time-average curve, whereas the field was normally set where the potassium resonance pulsed highest on the electrometer. All the observations used for the final analysis were made when the Bevatron was off. It was also necessary to omit many of the lower-field lines from the analysis because interference from higher-order multiple-quantum transitions made it impossible to choose center frequencies for the double-quantum transitions.

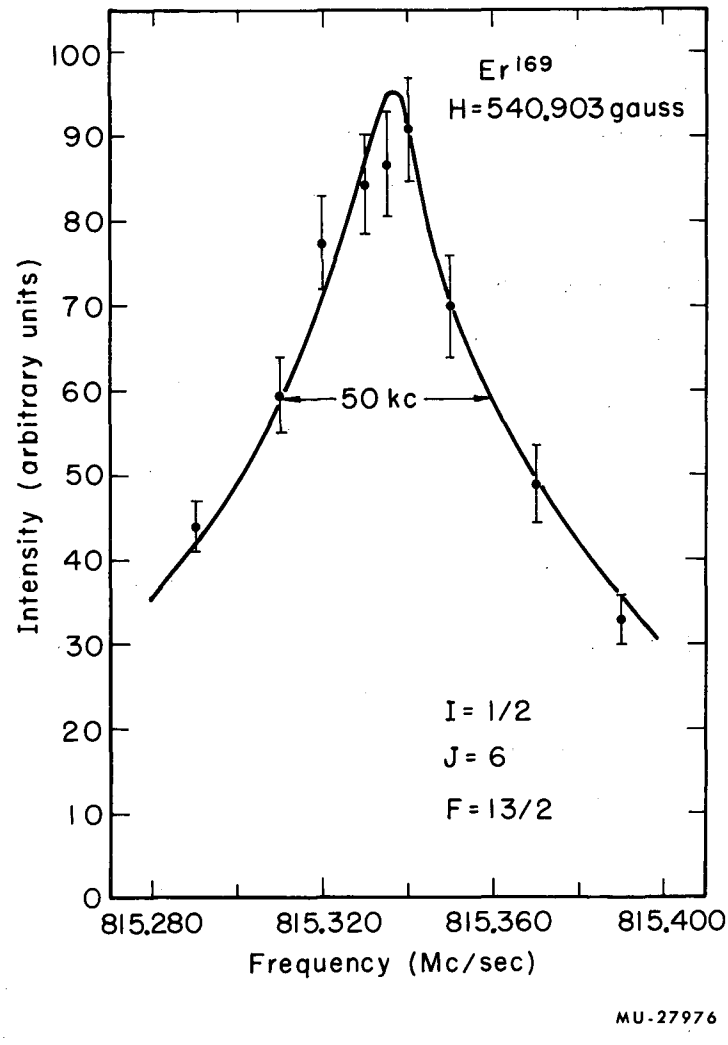

Fig. 5. Sample Er^{169} resonance.

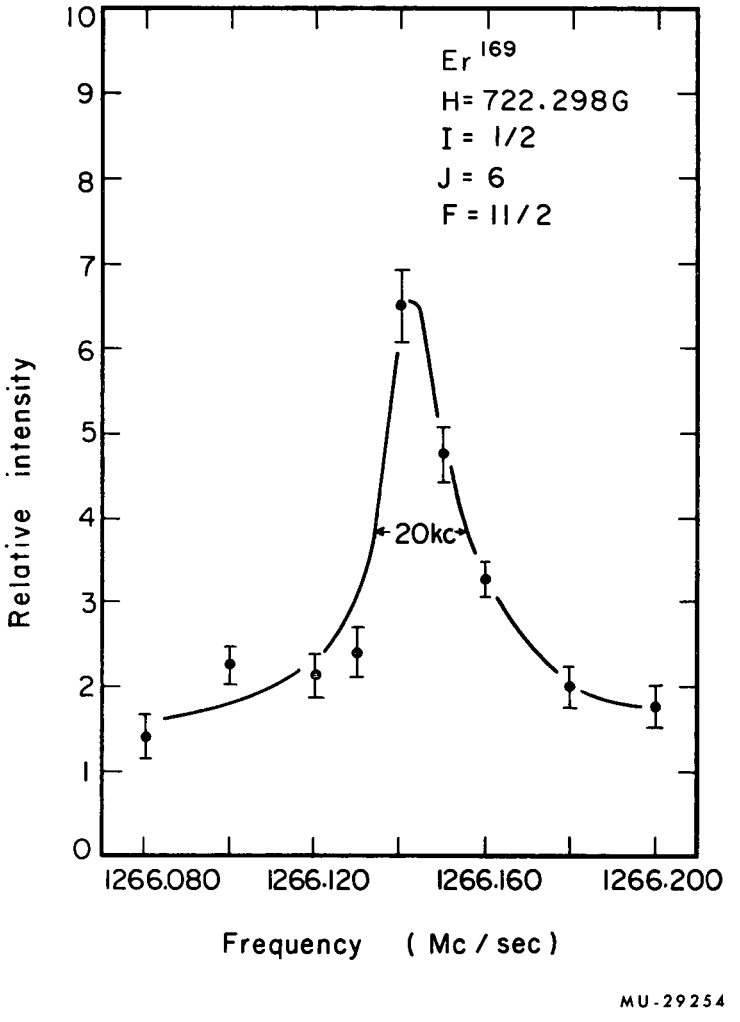

Fig. 6. Sample Er^{169} resonance.

Table I. Comparison of the observed frequencies with the frequencies predicted from the Hamiltonian (in Mc) $725.46\ \overline{I}\cdot\overline{J} + 1.16381\ \mu_0\ \overline{J}\cdot\overline{H} - 5.55 \times 10^{-4}\ \mu_0\ \overline{I}\cdot\overline{H}$.

Field (G)	Predicted frequency (kc)	Observed frequency (kc)	Residual (kc)	Transition
467.595	704496.5	704499.0(4.0)	2.5	F = 13/2
504.329	760020.2	760020.0(4.0)	-0.2	F = 13/2
540.903	815336.0	815332.0(4.0)	-4.0	F = 13/2
540.903	815336.0	815336.0(2.4)	0.0	F = 13/2
613.698	925539.9	925533.0(4.0)	-6.9	F = 13/2
649.962	980996.1	980995.0(2.4)	-1.1	F = 13/2
686.158	1035387.7	1035388.0(2.4)	0.3	F = 13/2
722.298	1090232.4	1090237.0(2.4)	4.6	F = 13/2
722.298	1090232.4	1090235.0(4.0)	2.6	F = 13/2
758.390	1145044.8	1145044.0(2.4)	-0.8	F = 13/2
794.442	1199836.1	1199835.0(2.4)	-1.1	F = 13/2
196.279	344409.4	344411.0(5.6)	1.6	F = 11/2
317.719	557484.5	557480.0(5.6)	-4.5	F = 11/2
467.595	820293.9	820290.0(4.0)	-3.9	F = 11/2
467.595	820293.9	820292.0(8.0)	-1.9	F = 11/2
504.329	884665.7	884666.0(2.4)	0.3	F = 11/2
540.903	948736.7	948735.0(5.6)	-1.7	F = 11/2
577.351	1012564.7	1012567.0(2.4)	2.3	F = 11/2
613.698	1076191.7	1076190.0(2.4)	-1.7	F = 11/2
649.962	1139648.9	1139650.0(2.4)	1.1	F = 11/2
686.158	1202960.0	1202959.0(2.4)	-1.0	F = 11/2
722.298	1266142.9	1266143.0(2.4)	0.1	F = 11/2
794.442	1392177.4	1392180.0(4.0)	2.6	F = 11/2

A good test of our data is the degree to which they fit the energy levels of the system by use of the final values of a, g_I, and g_J. This reflected in the χ^2 value. Here χ^2 is the weighted sum of the squares of the residuals in which the residual for an observation is the experimental frequency minus the calculated frequency. If χ^2 is equal to the number of data points minus the number of variables, the errors quoted in the input are of the order of a standard deviation for the distribution of possible frequency measurements.

It would be possible to obtain a good fit even with erroneous information if the data contained systematic errors of a kind that would produce the same effect as would a change in one of the parameters. A possible error of the type would be one that is linear in the field:

$$\mathcal{H}_{ext} = -g_I \overline{I}\cdot\overline{H}(1+a) - g_J\overline{J}\cdot\overline{H}(I+a) . \qquad (17)$$

Contributions to a could come from such effects as Doppler shift or dependence of the effective C field on oven position. The expression for the nonrelativistic Doppler shift is $\delta\nu/\nu = (v/c)\cos a$[16] where $\cos a = 1$ for radiation propagating parallel to the beam and, in our case, $v \approx 600$ m/sec. Thus $\delta\nu/\nu \leq 2 \times 10^{-6}$. White has investigated the effect of oven position by placing potassium in the rear oven and comparing transition frequencies. No shift was observed. The contributions to the measured g_I from the above two effects are clearly negligible; it would seem, however, that an additional uncertainty should be assigned to g_J to account for the possibility of errors linear in the field, and we will thus quote $g_J = -1.16381(5)$.

A pseudo $\overline{I}\,\overline{H}$ term might be introduced into the Hamiltonian through mixing of the fine-structure levels by the hyperfine-structure interaction. This would appear in the first order as a change in g_F. The $F = \frac{13}{2}$ hyperfine level occurs only in the $^3H_6$ electronic state so that the wave function is unperturbed, and the usual expression for g_F holds:

$$g_F\left(\frac{13}{2}\right) = g_J \frac{F(F+1)+J(J+1)-I(I+1)}{2F(F+1)} + g_I \frac{F(F+1)+I(I+1)-J(J+1)}{2F(F+1)} .$$

On the other hand, the electronic wave function for the $F = \frac{11}{2}$ level is

$$\left|\frac{11}{2}\right\rangle = \frac{1}{\sqrt{1+a^2}} \left|{}^3H_6\right\rangle + \frac{a}{\sqrt{1+a^2}} \left|{}^3H_5\right\rangle ,$$

where (18)

$$a = \frac{\left\langle {}^3H_6, \frac{11}{2} \left| -\bar{\mu}_n \cdot \bar{H}_e \right| {}^3H_5, \frac{11}{2} \right\rangle}{\Delta E_{J, J'}} .$$

The fine-structure separation is $\Delta E = 3a_{4f} \approx 7500\ cm^{-1}$, where a_{4f} is obtained from Judd and Lindgren, and the off-diagonal hfs matrix element is certainly less than or of the same order as the diagonal element $\frac{a}{2} K \approx 2500$ Mc. Thus $a \leq 10^{-5}$. We shall calculate the diagonal matrix element of $\mathcal{H}_{ext}$ in the F, m_F representation

$$W_{ext}\left(\frac{11}{2}\right) = \left\langle F = \frac{11}{2},\ m_F \left| (-\bar{\mu}_e - \bar{\mu}_n) \cdot \bar{H}_0 \right| F = \frac{11}{2},\ m_F \right\rangle$$

$$= -\left\langle \frac{11}{2} \left|\left| \bar{\mu}_e + \bar{\mu}_n \right|\right| \frac{11}{2} \right\rangle m_F H_0 \qquad (19)$$

$$= -g_F \mu_0 m_F H_0 .$$

Here we have used the Wigner-Eckart theorem with the reduced matrix element defined as in Condon and Shortly.[17] The customary definition of g_F has been used:

$$g_F = \frac{1}{\mu_0} \left(\frac{\mu F}{F}\right).$$

Continuing,

$$\mu_0\, g_F\left(\frac{11}{2}\right) = \frac{1}{1+a^2}\left\langle I \left\| \bar{\mu}_n \right\| I \right\rangle [2I+1]\, W(I, F, I, F;\, J=6,\, 1)$$

$$+ \frac{1}{1+a^2}\left\langle J=6 \left\| \bar{\mu}_e \right\| J=6 \right\rangle [2(J=6)+1]\; W(J=6,\, F,\, J=6,\, F;\, I,\, 1)$$

$$+ \frac{2a}{1+a^2}\left\langle \frac{11}{2},\ {}^3H_6 \left\| \bar{\mu}_e \right\| \frac{11}{2},\ {}^3H_5 \right\rangle + \theta(a^2) \tag{20}$$

$$= [g_F(J=6) + \delta g_F]\, \mu_0\,,$$

where $g_F(J=6)$ is the unperturbed g factor, W(abcd; ef) is a Racah coefficient,[18] and

$$\delta g_F \approx 2a \left\langle \frac{11}{2},\ {}^3H_6 \left\| \bar{L} + 2\bar{S} \right\| \frac{11}{2},\ {}^3H_5 \right\rangle$$

$$= 2a[(2J'+1)(2J+1)]^{1/2}\; W(J, F, J', F;\, I, 1) \times \left\langle J'=6 \left\| \bar{S} \right\| J=5 \right\rangle \tag{21}$$

$$\approx 2a[143]^{1/2} \left(\frac{1}{100}\right)\left(\frac{1}{6\sqrt{2}}\right)$$

The value of the reduced matrix element was obtained from Condon and Shortley,[17] p. 66. Substituting for a, we find $\delta g_F \leq 3 \times 10^{-7}$, which is completely negligible for our purposes.

D. Magnetic Moment Inferred from A

The magnetic moment can be obtained from the measured interaction constant by use of the relation

$$\mu_I = -IJ\, a / \langle H_{e,z} \rangle_{J,\, m_J = J} , \tag{22}$$

with

$$\langle H_{e,z} \rangle_{J,J} = -2\mu_0 \left\langle \frac{1}{r^3} \right\rangle \langle J, J | \sum_i \left\{ \ell_z - s_z + \frac{3z(\bar{s}\cdot\bar{r})}{r^2} \right\}_i | J, J \rangle .$$

Rather than assume pure L-S coupling, we shall write the $J = 6$ ground level of the configuration $(4f)^{12}$ as a mixture of contributions from the two terms ^3H and ^1I:

$$|J = 6\rangle = \frac{1}{\sqrt{1+a^2}} |^3H_6\rangle + \frac{a}{\sqrt{1+a^2}} |^1I_6\rangle . \tag{23}$$

Since there are only two terms involved, the value of a can be obtained by diagonalizing the energy matrix for $J = 6$. This calculation is performed in the appendix, and the result $a = 0.087$ is slightly different from that given by Judd and Lindgren.[19] The angular matrix element is most easily evaluated by writing the wave function in terms of single-particle coordinates. In the notation of Condon and Shortley,[17]

$$|^3H_6,\ m_J = 6\rangle = |3^+ 3^- 2^+ 2^- 1^+ 1^- 0^+ 0^- -1^+ -1^- -2^+ -3^+\rangle$$

and (24)

$$|^1I_6,\ m_J = 6\rangle = |3^+ 3^- 2^+ 2^- 1^+ 1^- 0^+ 0^- -1^+ -1^- -2^+ -2^-\rangle .$$

Thus,

$$\langle 6,6 | \sum_i | 6,6 \rangle = \frac{1}{1+a^2} \langle {}^3H_6 | \sum_i | {}^3H_6 \rangle + \frac{2a}{1+a^2} \langle {}^3H_6 | \sum_i | {}^1I_6 \rangle + \frac{a^2}{1+a^2} \langle {}^1I_6 | \sum_i | {}^1I_6 \rangle , \tag{25}$$

with

$$\langle {}^3H_6 | \sum_i | {}^3H_6 \rangle = \langle {}^3H_6 | \sum_i [\ell_{i,z} + s_{i,z}(3\cos^2\theta_i - 1)] | {}^3H_6 \rangle$$

$$= 2 + 3 + \frac{1}{2} \langle -2, -3 | \sum_i (3\cos^2\theta_i - 1) | -2, -3 \rangle$$

$$= 4.66 ,$$

$$\langle {}^1I_6 | \sum_i | {}^1I_6 \rangle = 3 + 3 = 6 ,$$

and

$$\langle {}^3H_6 | \sum_i | {}^1I_6 \rangle = \langle -3^+ | \frac{3}{2} \frac{z}{r^2} s_+ r_- | -2^- \rangle$$

$$= \langle -3 | \sin\theta\cos\theta e^{i\phi} | -2 \rangle = -0.27 ,$$

so that

$$\langle 6, 6 | \sum_i | 6, 6 \rangle = 4.62 . \qquad (26)$$

The single-particle matrix elements were evaluated with the aid of the expressions[17, 20]

$$\langle \ell \; s \; m_\ell \; m_s | (3\cos^2\theta - 1) | \ell \; s \; m_\ell \; m_s \rangle \qquad (27)$$

$$= - \frac{2}{(2\ell - 1)(2\ell + 3)} [3m_\ell{}^2 - \ell(\ell + 1)]$$

and

$$\left\langle \ell = 3,\ m_\ell + 1 \left| \cos\theta \sin\theta e^{i\phi} \right| \ell = 3,\ m_\ell \right\rangle$$

$$= -\left(\frac{1}{45}\right)(2m_\ell + 1)\left[(4 + m_\ell)(3 - m_\ell)\right]^{1/2} . \tag{28}$$

The above result differs by about 1% from that obtained in the Russell-Saunders approximation (i.e., $\alpha = 0$).

The earliest attempts to evaluate $\left\langle \frac{1}{r^3} \right\rangle$ were based on the assumption that the rare earths are characterized by simple hydrogenic wave functions.[21, 22, 23] In this approximation the spin-orbit parameter is given by

$$\rho_{n\ell} = \frac{(z-\sigma)e^2h^2}{2\mu^2c^2a^3}\left\langle \frac{1}{r^3} \right\rangle$$

$$= \frac{(z-\sigma)^4 e^2h^2}{2\mu^2c^2a^3} \frac{1}{h^3\ell(\ell+1/2)(\ell+1)} . \tag{29}$$

The second expression is fitted to the observed fine-structure data to obtain a value for the shielding parameter σ. The first expression then yields $\left\langle \frac{1}{r^3} \right\rangle$. Improving on the earlier work of Elliott and Stevens,[22] Bleaney[23] in 1955 worked out a set of $\left\langle \frac{1}{r^3} \right\rangle$ values for the triply ionized rare earths. He assigned an uncertainty of 5% to his values. In 1959, Ridley[24] obtained Hartree self-consistent-field wave functions for Pr^{3+} and Tm^{3+}. The resultant $\left\langle \frac{1}{r^3} \right\rangle$ values were considerably smaller than those of Bleaney. The next development was the evaluation of $\left\langle \frac{1}{r^3} \right\rangle$ by Judd and Lindgren,[19, 25] who used the analytic wave function

$$R \approx r^n e^{-ar} \cosh\left[K(ar-n)\right] , \tag{30}$$

where n is the principal quantum number, and K and a are parameters. K was evaluated by finding the best fit to Ridley's Pr^{3+} and Tm^{3+} wave functions. With the assumption of a linear dependence on Z, a was determined for each ion or atom by fitting the observed fine-structure separations and by using

$$\rho = C \left\langle \frac{1}{r} \frac{dV}{dr} \right\rangle H_r , \tag{31}$$

where H_r is a relativistic correction and V is evaluated either by substituting R in the Schroedinger equation or by using the Thomas-Fermi model.[17] The results for the ions again differ from Bleaney's by 15 to 25% with an estimated accuracy of 5%. Most recently, Freeman and Watson have performed nonrelativistic Hartree-Fock calculations for the rare earth ions and have obtained $\left\langle \frac{1}{r^3} \right\rangle$ values within 5% of Bleaney's.

Small admixtures of configurations having unpaired s electrons can have a considerable effect on the measured interaction constant.[20] The electrons may still couple to the ground state $^3H_6$ leaving g_J unaltered, but will have a net spin density at the nucleus and hence a contact interaction. Although quantitative calculations have not been performed, the magnitude of the effect has been estimated by Bleaney on the basis of an analogue with the iron-group and hyperfine-structure measurements in the ^8S term of E_u^{2+} and G_d^{3+}, where a vanishes in the absence of perturbations.[23] He believes the effect to be less than 6% for the rare earth ions and, in particular, quotes a value of $\pm 1.4\%$ for E_r^{3+}. Since the hfs of the E_u atom is smaller than that of E_u^{3+}, the effect may be even smaller in the atomic case.

If Lindgren's $\left\langle \frac{1}{r^3} \right\rangle$ value of 9.84 atomic units (au) is used, we obtain $\mu_I = 0.504(50)$ nm for the moment inferred from A. The 10% uncertainty is assigned to cover the effects of configuration mixing and the quoted uncertainty in $\left\langle \frac{1}{r^3} \right\rangle$.

Table II. Measured nuclear-magnetic moments compared with those obtained from hfs data by using the $\left\langle \frac{1}{r^3} \right\rangle$ values of Bleaney, Lindgren, and Freeman and Watson. The Nd^{143} inferences are based on Halford's hfs result[27] $g_n\left\langle \frac{1}{r^3} \right\rangle = (-11.88 \pm 0.12) \times 10^{24}$ cm^{-3}. For Yb^{171}, we have used Low's paramagnetic-resonance result.[30] The moments usually found in the literature are based on earlier less-accurate work.[31] The various inferred moments also appear to be inconsistent. All units are nuclear magnetons.

	$(Nd^{143})^{3+}$	Er^{169}	Tm^{169}	$(Yb^{171})^{3+}$
Bleaney	-0.99	--	--	0.41
Lindgren	-1.26	0.504	-0.24	0.49
Freeman and Watson	-1.02	--	--	0.43
Measured	-1.076 (60)	0.513 (25)	-0.229 (3)	0.4930 (4)
References	27		28	29, 30

E. Conclusions

Recently, directly measured nuclear moments have been reported for Nd^{173}, Tm^{169}, and Yb^{171}.[27,28,29] These moments are summarized in Table II along with the present result and the values inferred from hfs data by using the various $\left\langle \frac{1}{r^3} \right\rangle$'s.[27,30,31] Our result includes a correction for the breakdown of Russell-Saunder coupling. The $\left\langle \frac{1}{r^3} \right\rangle$ values of Lindgren appear to give reasonably good agreement with experiment for the heavier lanthanides, while the neodymium result is less conclusive and would seem to favor the work of Freeman and Watson. The good agreement achieved for the heavier lanthanides tends to substantiate the belief that the effects of configuration mixing are small.

Er^{169} lies in a region of extreme nuclear deformation. Individual particle wave functions for such nuclei have been worked out by

Nilsson and are discussed more fully later.[32] Nilsson gives the following expression for the magnetic moment of a nucleus with spin $I = 1/2$ and odd parity

$$\mu = \frac{1}{3}\left\{(g_\ell - g_R)d - \frac{1}{2}g_s + g_\ell + g_R\right\}. \tag{32}$$

The g factors are written here in terms of the nuclear magneton

$$g_\ell = 0, \quad g_s = -3.83, \quad \text{and} \quad g_R = \frac{Z}{A} = 0.40 .$$

To follow Mottelson and Nilsson, we assume that the 101 st neutron is characterized by the state $\frac{1}{2}^- |521\rangle$ and by the decoupling parameter $d = 0.87$, with the result that $\mu = 0.65$ nm.[33] Our measured value, $\mu = 0.513(25)$ nm, is somewhat lower than this but is consistent with measurements on other similar nuclei.

It is interesting to note that the expression given above for the nuclear moment depends only on the decoupling parameter and not explicitly on the form of the nuclear wave function. This is a peculiarity of $I = 1/2$, odd-parity nuclei -- the moments of which are largely independent of deformation.[34] The observed values are grouped quite closely around $\mu = +0.5$ nm for odd neutrons, and the discrepancy between these values and the theoretical predictions is usually attributed to a quenching of the intrinsic magnetic moment of the neutron within the nucleus.[35]

IV. SPINS OF REFRACTORY GROUP NUCLIDES

A. Introduction

The elements with atomic numbers 71 through 78 are often referred to as "the refractories." The term stems from their high melting points -- ranging from 1700°C for hafnium to 3370°C for tungsten -- and low chemical activity. Little vapor-pressure information is available, but the pressure just below the melting point is probably of the order of a hundredth of a millimeter for tungsten and tantalum and considerably less for hafnium.[36]

The electronic properties of the refractories have been studied by optical spectroscopy, and in particular the energy levels and g factors have been determined.[37] The g factors of the levels of interest to us are listed in Table III. These are known with relatively poor accuracy (about 1% for tungsten and iridium), and improvements would serve to test the applicability of Russell-Saunders coupling and the importance of relativistic and diamagnetic corrections. The nuclear properties are especially interesting, since the refractory region is characterized by considerable nuclear deformation. The spins and moments of the lighter nuclides should provide a test of the strong deformation model, while the properties of the heavier nuclides will indicate to what extent this model breaks down and the spherical shell model becomes more applicable.

Although the aim of the present work has been the determination of the nuclear spins of as many of the radioactive nuclides in the refractory group as possible, plans are being made to extend the investigations to the measurements of hfs constants and electronic g factors.

An interesting possibility for an experiment arises from the competition in the region between two configurations, one of which has an unpaired s electron. In tungsten and iridium, the lowest level of the excited $d^{n+1}s$ configuration lies only slightly above the $d^n s^2$ ground level and is sufficiently populated to be studied by atomic beams. The hfs anomaly ${}^{\alpha}\Delta^{\beta}$ between the isotopes α and β is defined as[4]

Table III. Summary of electronic levels studied

Element	Configuration	State	Observed g_J
Tantalum	$(5d)^3(6s)^2$	$^4F_{3/2}$	-0.447
		$^4F_{5/2}$	-1.031
		$^4F_{7/2}$	-1.218
Tungsten	$(5d)^4(6s)^2$	$^5D_1$	-1.51
		$^5D_2$	-1.48
		$^5D_3$	-1.50
		$^5D_4$	-1.49
	$(5d)^5(6s)$	$^7S_3$	-1.98
Rhenium	$(5d)^5(6s)^2$	$^6S_{5/2}$	-1.950
Iridium	$(5d)^7(6s)^2$	$^4F_{9/2}$	-1.30
	$(5d)^8(6s)$	$^4F_{9/2}$	-1.33

$$ {}^{\alpha}\Delta^{\beta} = \frac{(a^{\alpha}/a^{\beta})}{(g_I^{\alpha}/g_I^{\beta})} - 1 \, . \qquad (33) $$

The anomaly is zero if the electronic wave function vanishes within the nucleus, and is appreciable only for s and $p_{1/2}$ electrons. Thus, we can measure ${}^{\alpha}\Delta^{\beta}$ for the excited configuration of tungsten or iridium without directly measuring the g factors, since $(g_I^{\alpha}/g_I^{\beta}) = (a^{\alpha}/a^{\beta})$ for the ground configuration.

B. Experimental Method

Past attempts to make atomic beams of the refractory metals have been unsuccessful because the high melting points and low vapor

pressures have made the use of conventional ovens impossible. We have overcome this problem by directly heating a narrow source by electron bombardment. The source mount, partially disassembled, is shown in Fig. 7. The filament is grounded, and the source is at a positive potential of the order of 1000 V. Satisfactory results have been obtained by using both 0.010-in.- and 0.020-in.-diam wire sources. The use of a wire source, in addition to being the only method available for production of a refractory beam avoids many of the difficulties encountered with ovens: such as arcing, creep, and interaction between the oven materials and the sample. It is necessary, however, to have a sufficient specific activity to yield a usable beam. Fortunately the refractories are characterized by very high cross sections for thermal neutron capture.

All the refractories except osmium are available in forms suitable for our use, and satisfactory results have been obtained with tantalum, tungsten, rhenium and iridium. Attempts were made to obtain a beam of hafnium, but the vapor pressure below the melting point proved to be insufficient.

The transition frequencies in the Zeeman region are dependent on I, J, F, g_I, and g_J:

$$\nu = -g_F \frac{\mu_0 H}{h}$$

with

$$g_F = g_J \frac{F(F+1)+J(J+1)-I(I+1)}{2F(F+1)} + g_I \frac{F(F+1)+I(I+1)-J(J+1)}{2F(F+1)} .$$

The various J and g_J values are known; the term in g_I is small and for our purposes may be neglected. A spin search generally consists of a set of exposures at frequencies corresponding to the various possible combinations of I, J, and F and is made at least at two different magnetic fields in order to avoid a fortuitous fit. The spin is integral or half integral, depending on whether the total number of nucleons is even or odd.

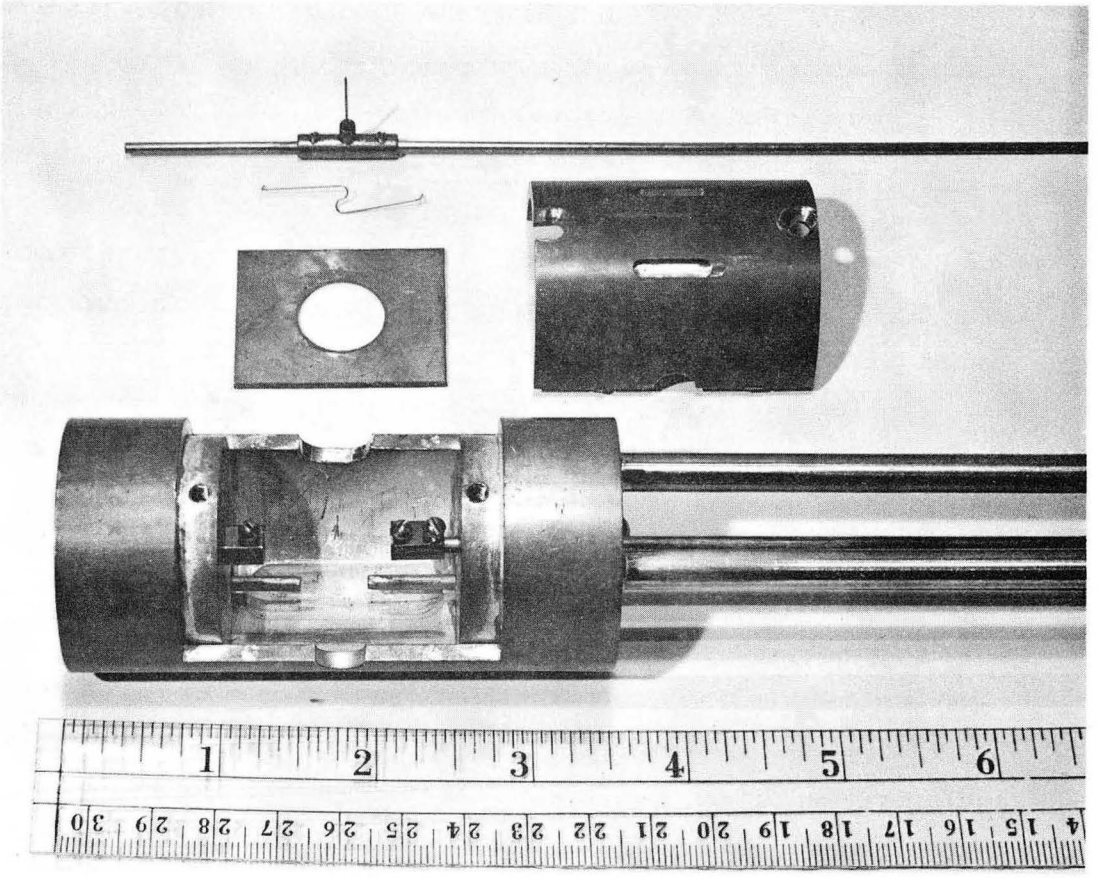

ZN-3574

Fig. 7. Source mount with refractory sample.

C. Tungsten

Tungsten, with a melting point of 3640°K, is the most refractory of metals and, as such, was the first one to which the wire technique of beam production was applied. About 1 Ci of the 24-h isotope W^{187} was produced by bombarding 5/8-in. of 0.010-in.-diam wire with thermal neutrons at 10^{14} neutrons/cm^2/sec in the General Electric test reactor. Calculations indicated that a vapor pressure of 0.01 mm should be sufficient to yield a counting rate of several thousand counts/min on a 1-min full-beam exposure. In practice, beams of about 1000 counts/min were found to last from 3 to 4 h.

The low-lying electronic levels in tungsten are shown in Table IV. At our high operating temperatures, one would expect both configurations to be present in sufficient abundance for study. The populations shown were calculated by using a temperature of 3600°K.

Data were taken at two values of magnetic field (Figs. 9 and 10), and the nuclear spin of W^{187} was found to be $I = 3/2$. The notation used in labeling transitions is "I(JF)," where "a" corresponds to $F = F_{max}$, etc. as indicated in Fig. 8, and "exc" refers to the excited configuration d^5s. The low points correspond to other values of nuclear spin. Resonances were observed in each of the electronic states listed in Table IV except the $J = 0$ ground state. Atoms in this state are not deflected sufficiently to be studied.

The 48-h bombardment used in the production of W^{187} yields only negligible quantities of other radioactive isotopes. Both the full-beam and resonance foils decayed with a strict 24-h half life (Fig. 11).

Tungsten-185 was produced by bombarding 0.020-in.-diam tungsten wire for about 70 days at a flux of 5×10^{14} neutrons/cm^2/sec in the Materials Test Reactor at Arco, Idaho. The samples were allowed to "cool" for at least 10 days before use to insure predominance of W^{185} over W^{187} and, in fact, the last observations were made more than 40 days after removal from the reactor. The results, Figs. 12 and 13, indicate a spin of $I = 3/2$. A typical resonance is shown in Fig. 14.

During the course of our work, it was observed that foils often would not re-count properly after completion of a run. This effect was

Table IV. Low-lying electronic levels in tungsten.[37]

Configuration	State	Energy (cm^{-1})	Observed g_J	Abundance (%)
$(5d)^4 (6s)^2$	$^5D_0$	0	--	11.5
$(5d)^4 (6s)^2$	$^5D_1$	1670.3	-1.51	17.5
$(5d)^4 (6s)^2$	$^5D_2$	3325.5	-1.48	15.3
$(5d)^4 (6s)^2$	$^5D_3$	4830.0	-1.50	11.7
$(5d)^4 (6s)^2$	$^5D_4$	6219.3	-1.49	8.7
$(5d)^5 (6s)$	$^7S_3$	2951.3	-1.98	34.7

attributed to the failure of the tungsten atoms to stick well on platinum, and proved an obstacle to obtaining satisfactory decay plots for W^{185}. The final curve, Fig. 15, was obtained by using a foil that had been painted with clear enamel after exposure.

Previous β-decay analysis had resulted in an assignment of $I = 1/2$ for W^{187} and $I = 3/2$ for W^{185}.[38] The former assignment is not consistent with our result.

D. Rhenium

The electronic structure of rhenium is characterized by a half-filled d shell, $(5d)^5$. The lowest term in this configuration has only one level $^6S_{5/2}$ with the measured g factor, $g_J = -1.950$. The next higher state $^4P_{5/2}$ lies at 11,580 cm^{-1} and was not observed in our experiment. Figure 16 shows the hfs energy levels for the system $I = 1$, $J = 5/2$.

The two rhenium isotopes studies were produced by bombardment of 0.010-in.-diam wires at 10^{14} neutrons/cm^2/sec. A 5-h

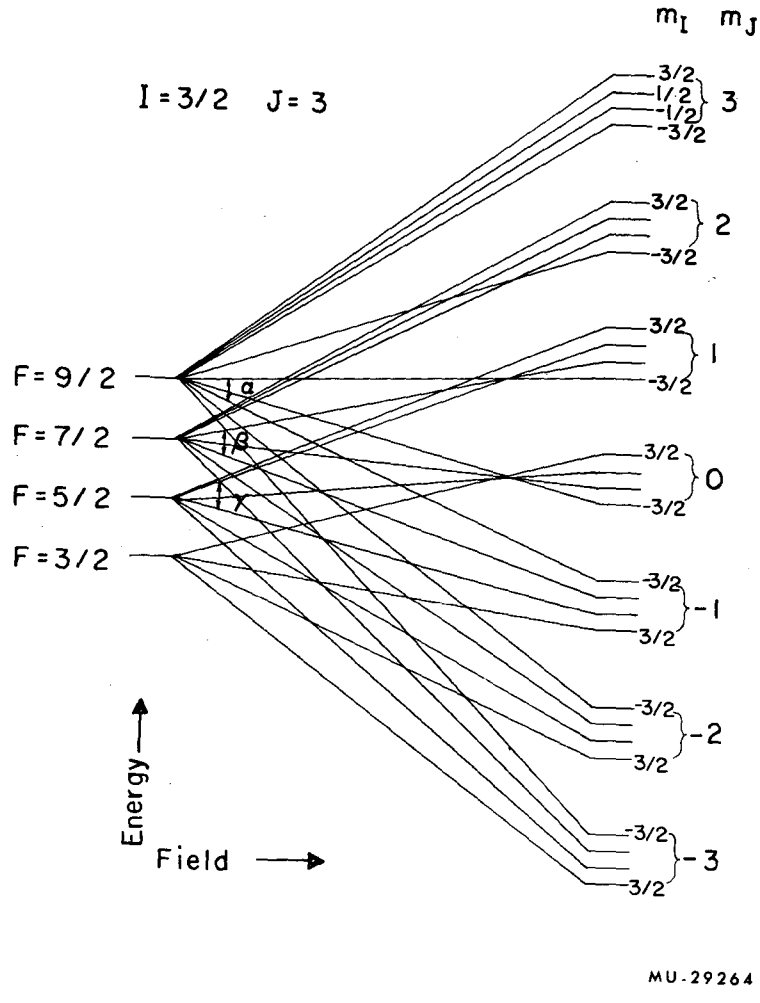

Fig. 8. Hfs levels of W^{185} and W^{187} in the "J = 3" electronic states (schematic).

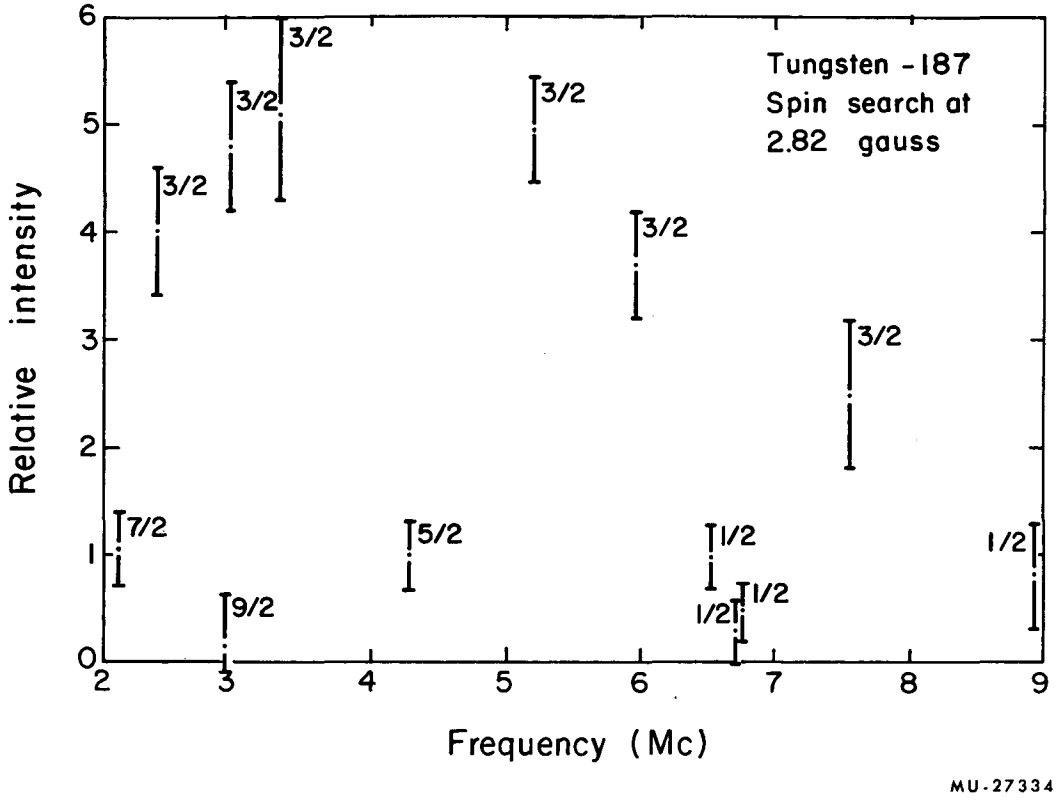

Fig. 9. W^{187} spin search.

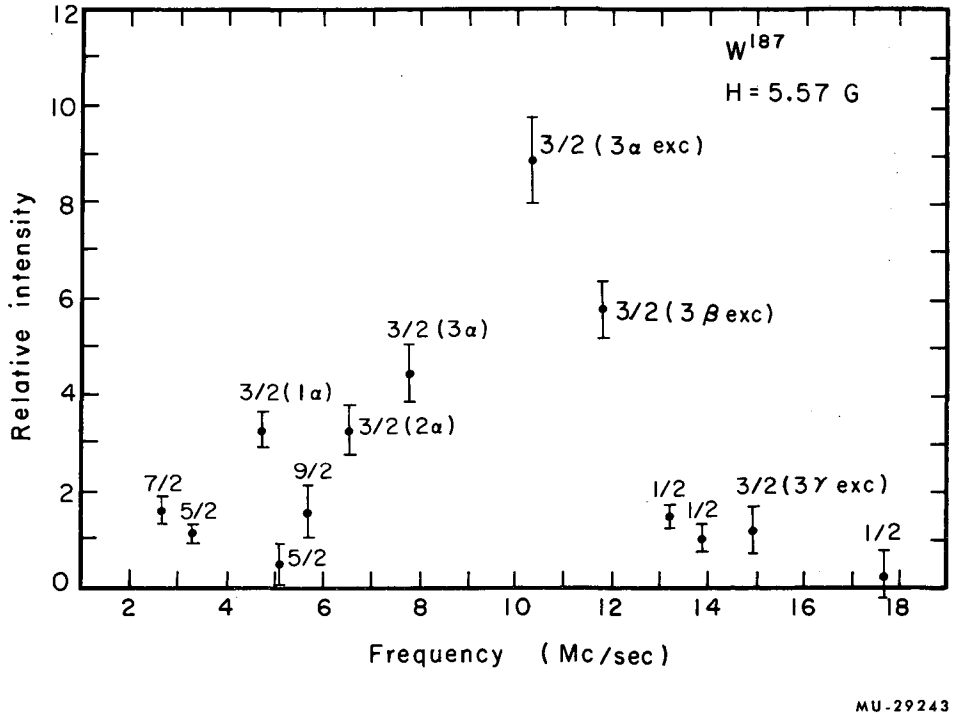

Fig. 10. W^{187} spin search.

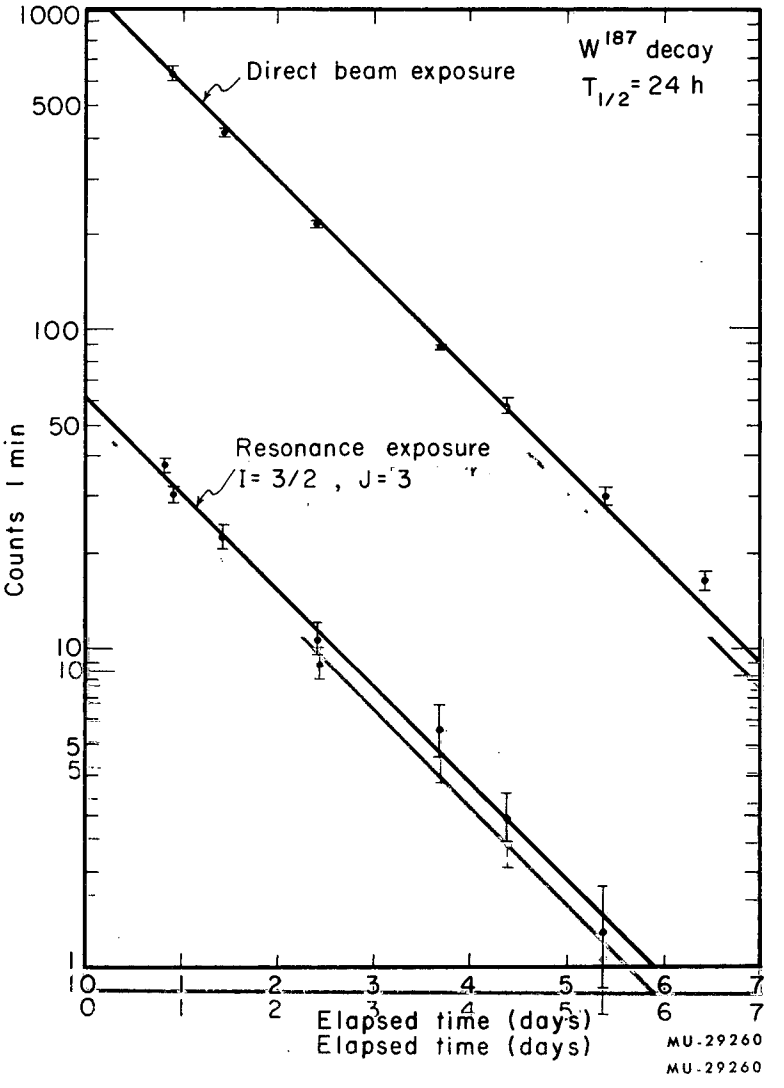

Fig. 11. Decay of W^{187} direct-beam and resonance foils.
Fig. 11. Decay of W^{187} direct-beam and resonance foils.

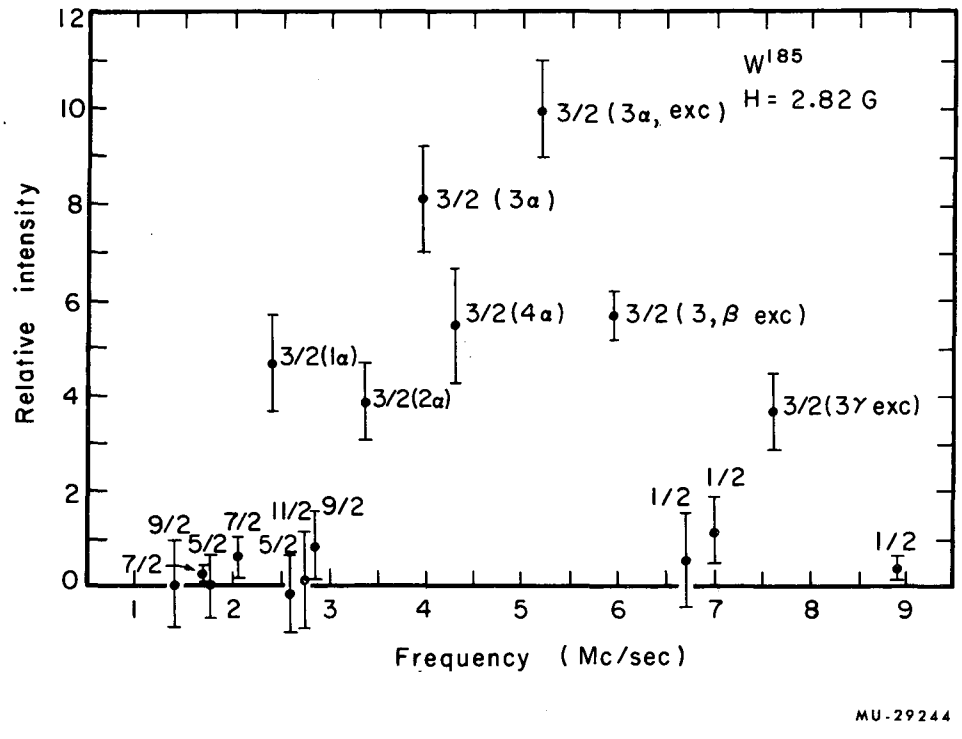

Fig. 12. W^{185} spin search.

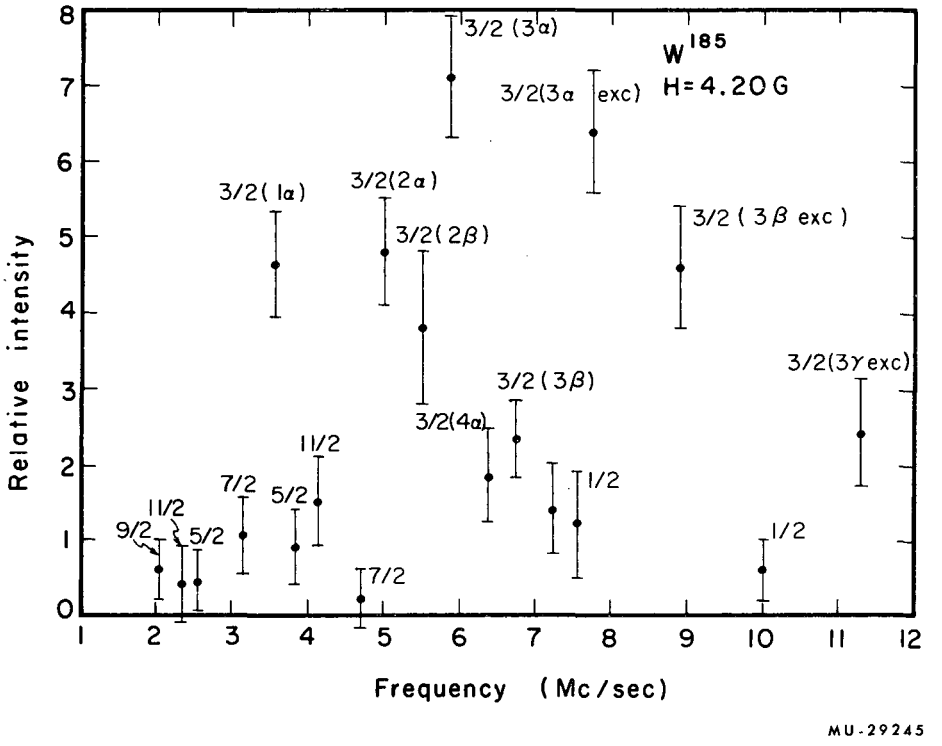

Fig. 13. W^{185} spin search.

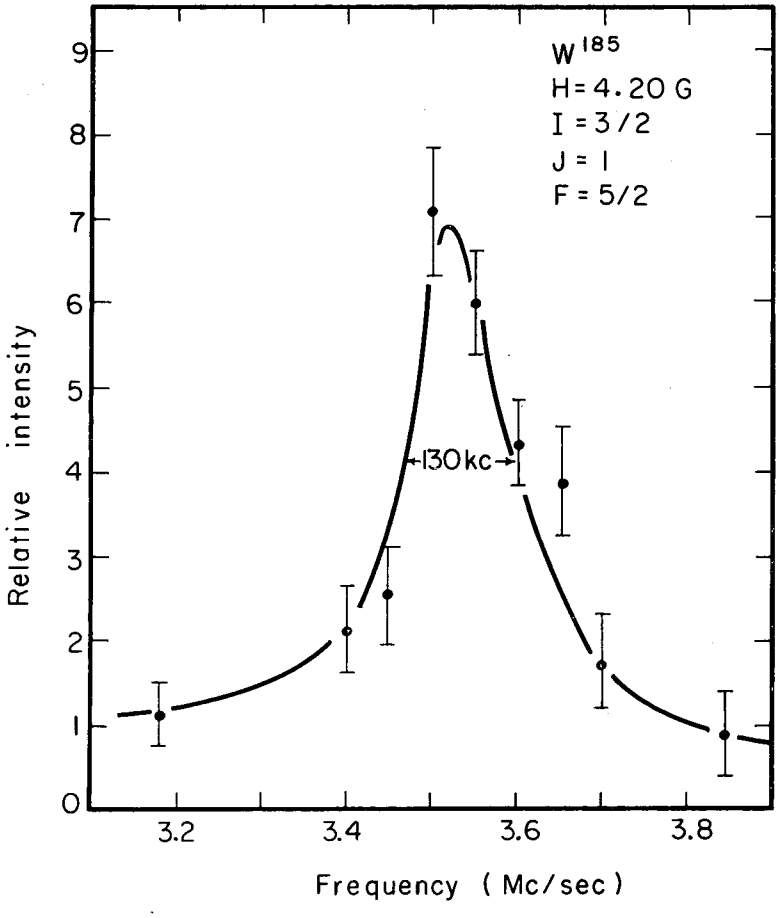

Fig. 14. Sample W^{185} resonance.

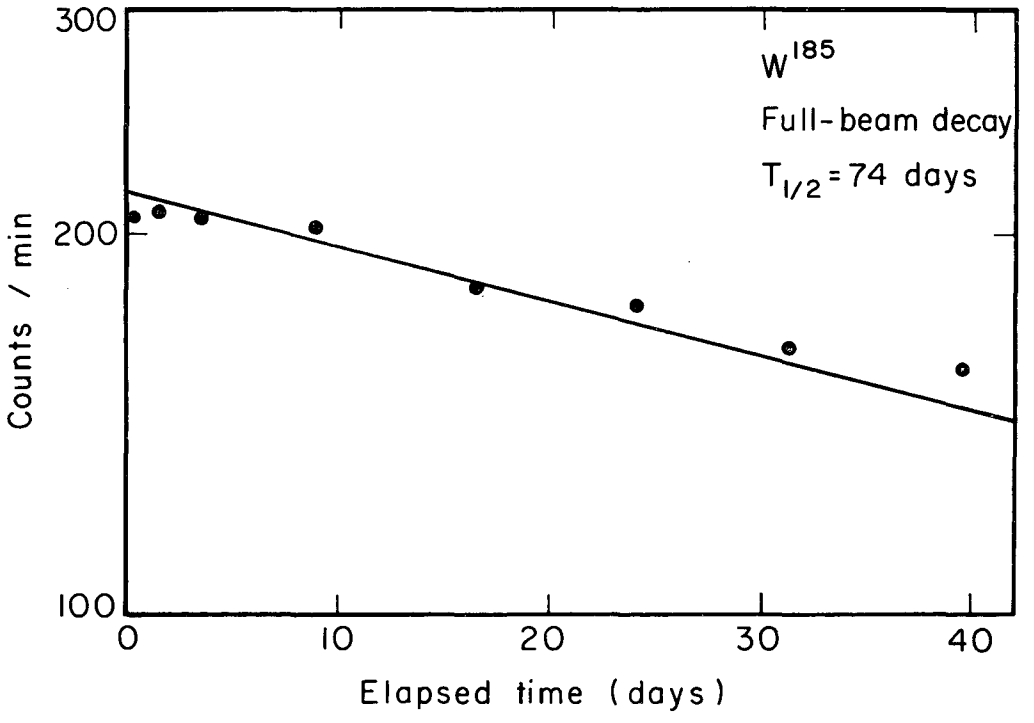

Fig. 15. W^{185} full-beam decay.

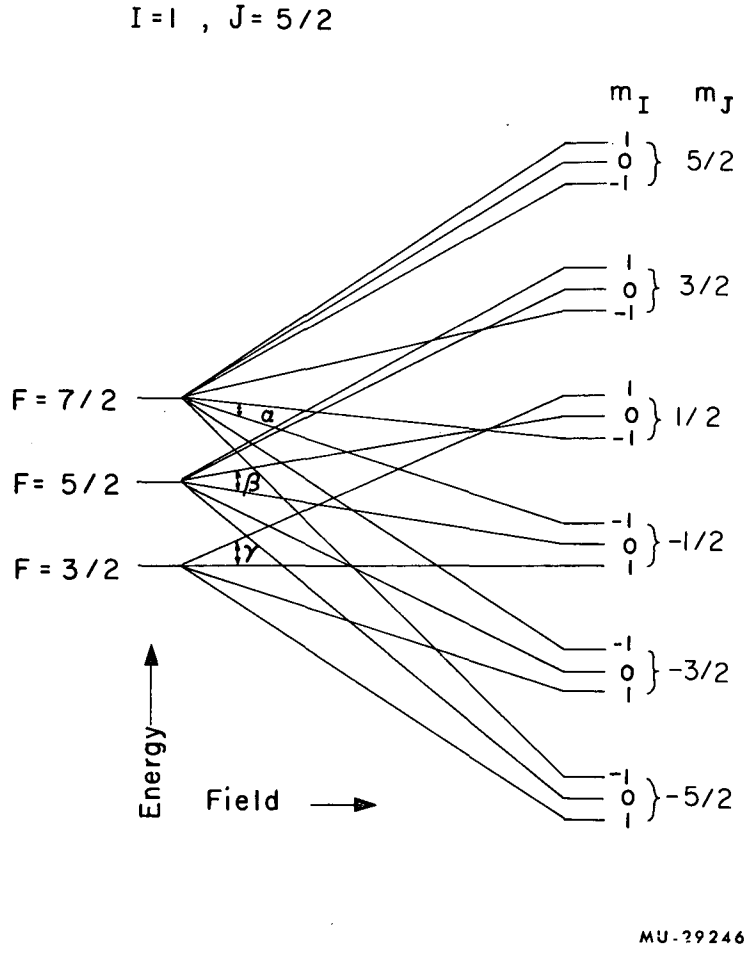

Fig. 16. Hfs levels of Re^{186} and Re^{188} (schematic).

bombardment yields about 1 Ci of rhenium-188 ($T_{1/2} = 17$ h) and 0.2 Ci of rhenium-186 ($T_{1/2} = 90$ h). Re^{186} is preferentially produced by bombarding the sample for 5 days and allowing a 7-day decay before use. This yields about 0.9 Ci with less than 1% Re^{188}.

The first runs were made by using the 5-h bombardment. The results, Figs. 17, 18, and 19, dictate a spin assignment of $I = 1$ for Re^{188}. The notation here is simply "I, F" since $J = 5/2$ for all points. Decay plots, Figs. 20 and 21, reveal that the proportion of Re^{186} in the full-beam and resonance exposures is about the same (20%) and thus suggest a spin of $I = 1$ for this isotope also. Runs made by using the longer bombardment confirmed this assignment, Figs. 22 and 23. Decay of a resonance foil is plotted in Fig. 24.

Since the $^6S_{5/2}$ ground-state wave function of rhenium is spherically symmetric, the expectation value of the field at the nucleus vanishes:

$$\left|{}^6S_{5/2},\ m_J = 5/2\right\rangle = \left|2^+1^+0^+\text{-}1^+\text{-}2^+\right\rangle , \tag{34}$$

and, using Eq. (27),

$$\left\langle {}^6S_{5/2}, \frac{5}{2}\right| \sum_i \left[\ell_z - s_z + \frac{3z(\bar{s}\cdot\bar{r})}{r^2}\right]_i \left|{}^6S_{5/2},\ \frac{5}{2}\right\rangle$$

$$= \left\langle \sum_i \left[\ell_z + s_z(3\cos^2\theta - 1)\right]_i \right\rangle \tag{35}$$

$$= 0 - \frac{2}{21} \sum_{m_\ell = -2}^{2} [3m^2 - 6] = 0 .$$

One would expect rhenium hyperfine-structure energies to be very small, since the only contributions come from configuration mixing and the break-down of Russell-Saunders coupling. This would be reflected in deviations from the Zeeman approximation at relatively low fields. Such has proved to be the case. Resonances in the two highest F states

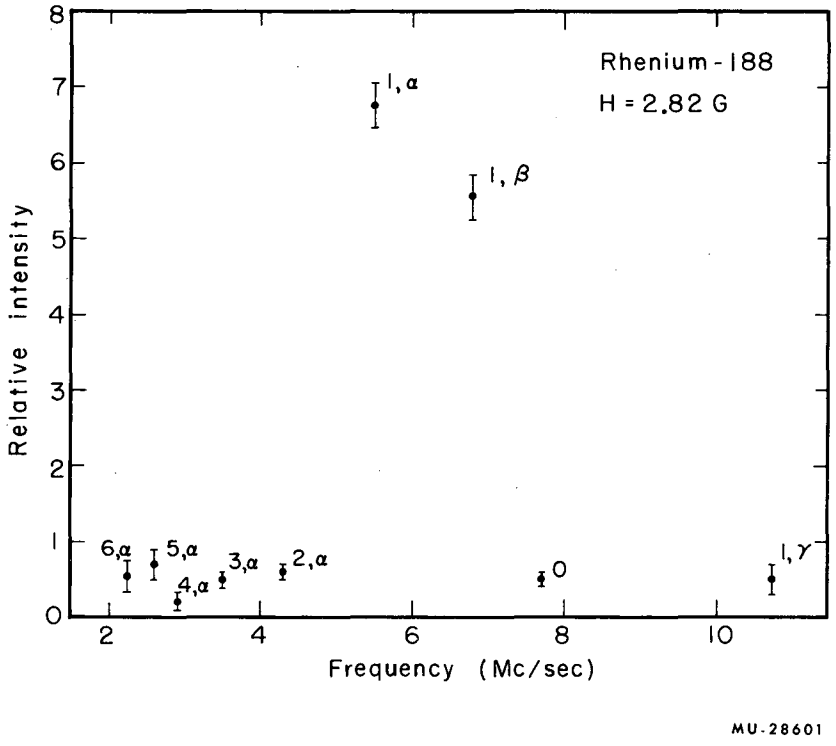

Fig. 17. Re^{188} spin search.

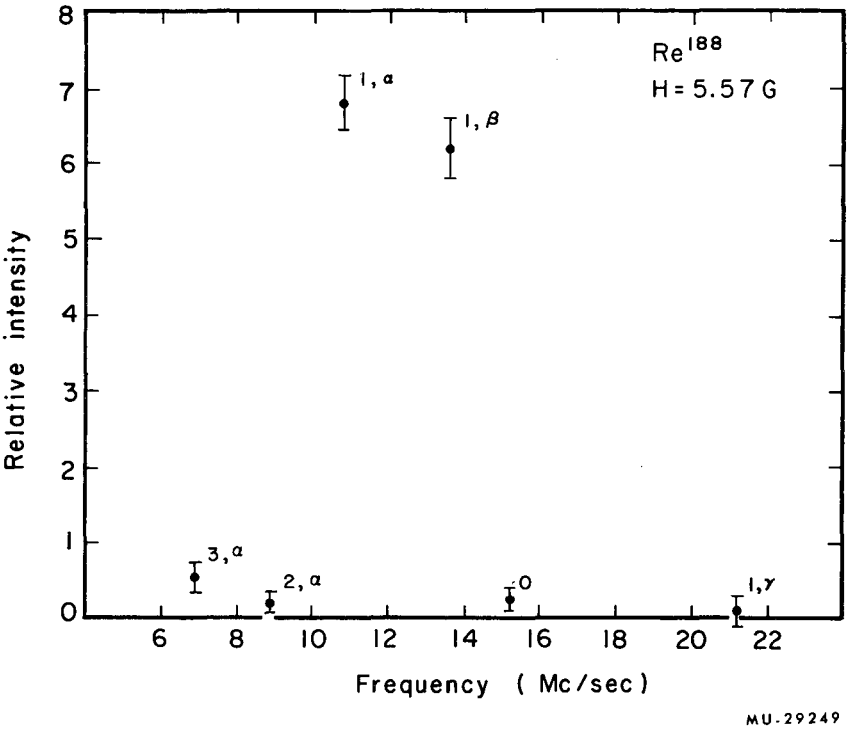

Fig. 18. Re^{188} spin search.

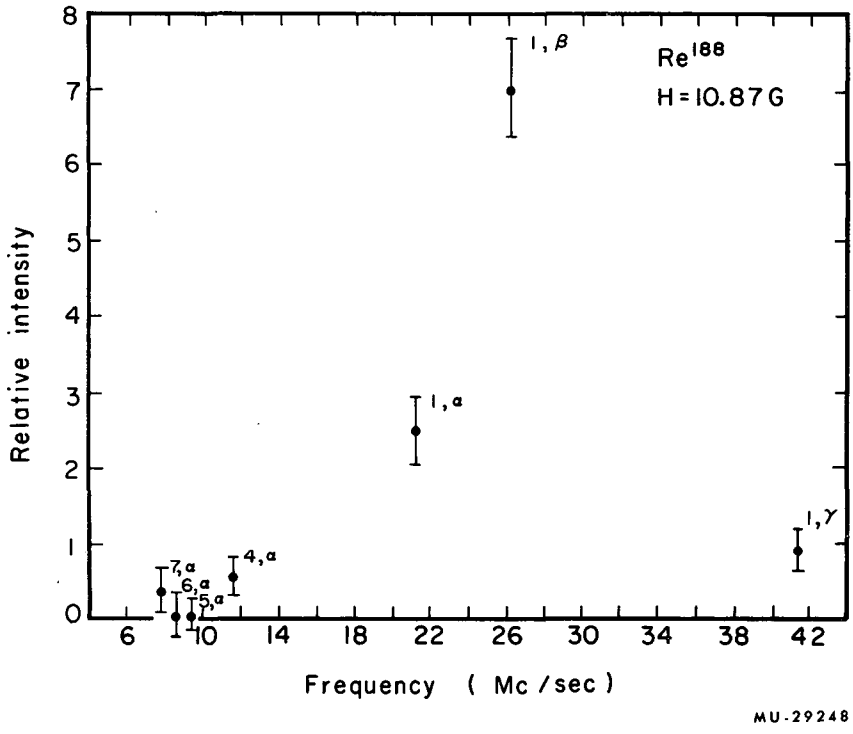

Fig. 19. Re^{188} spin search.

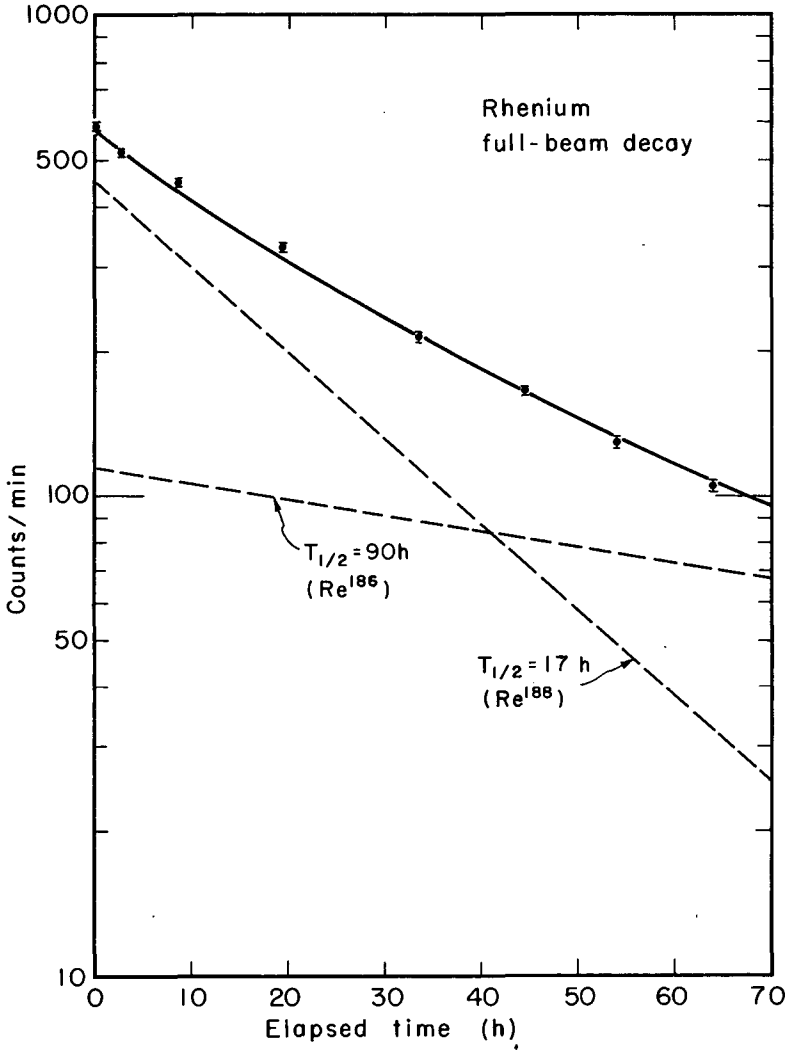

Fig. 20. Re^{188} full beam decay.

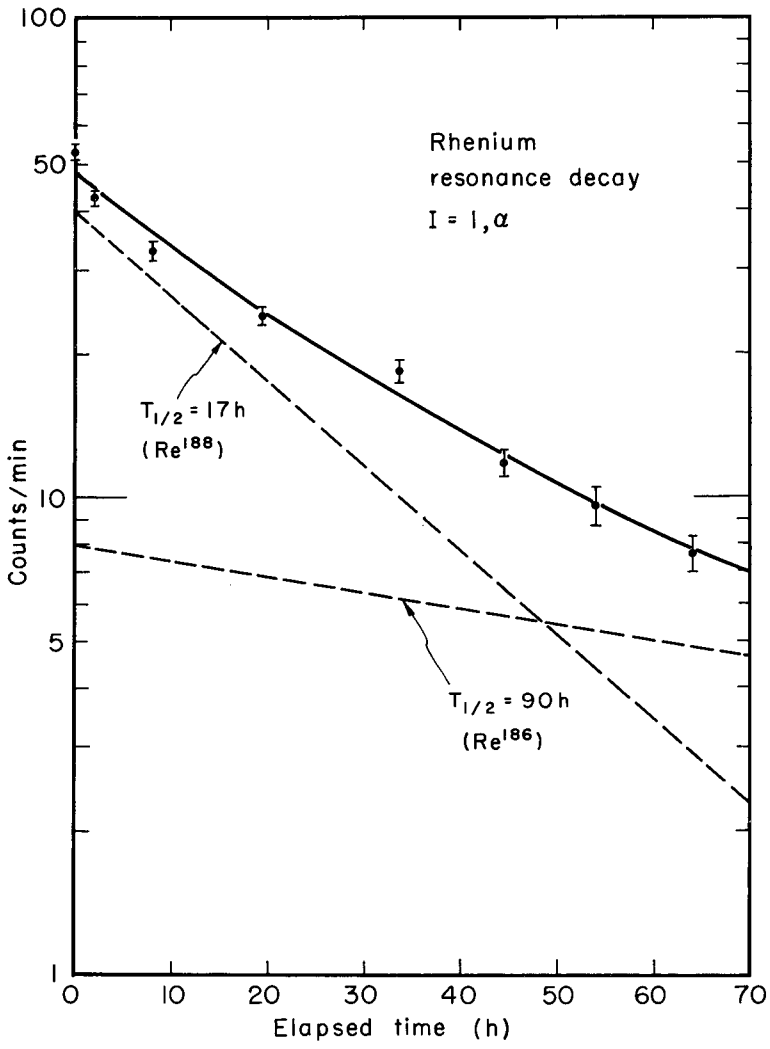

Fig. 21. Re^{188} resonance decay.

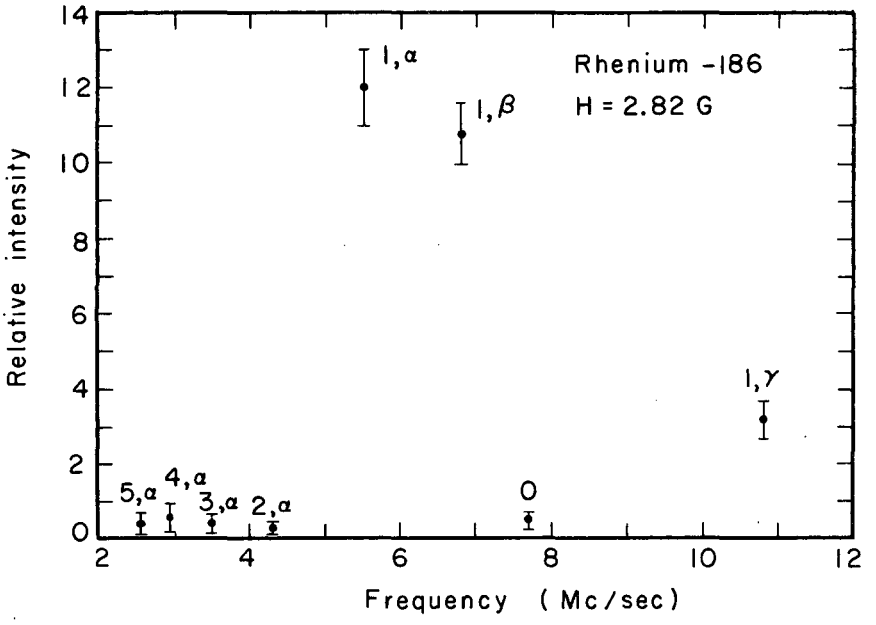

Fig. 22. Re^{186} spin search.

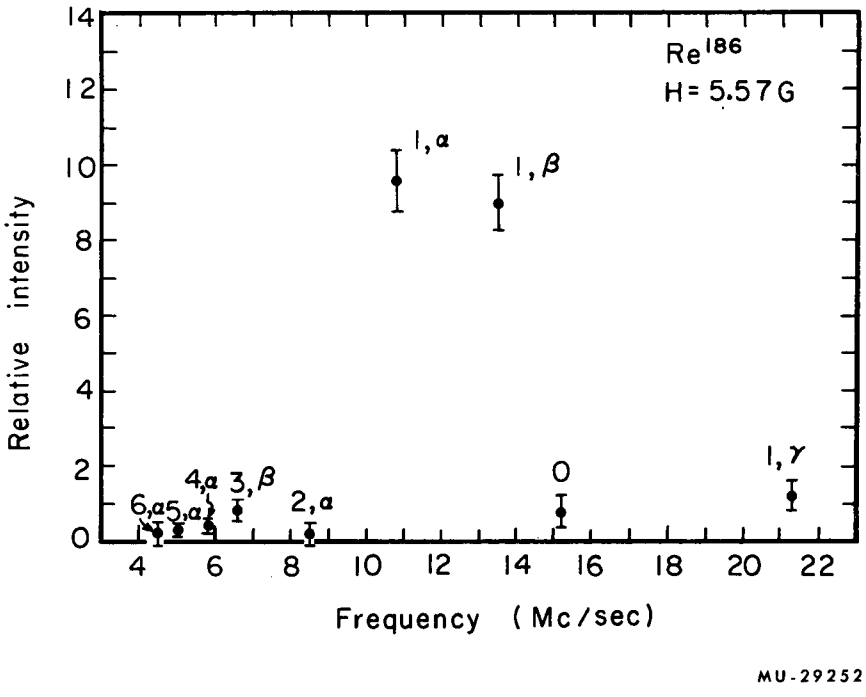

Fig. 23. Re^{186} spin search.

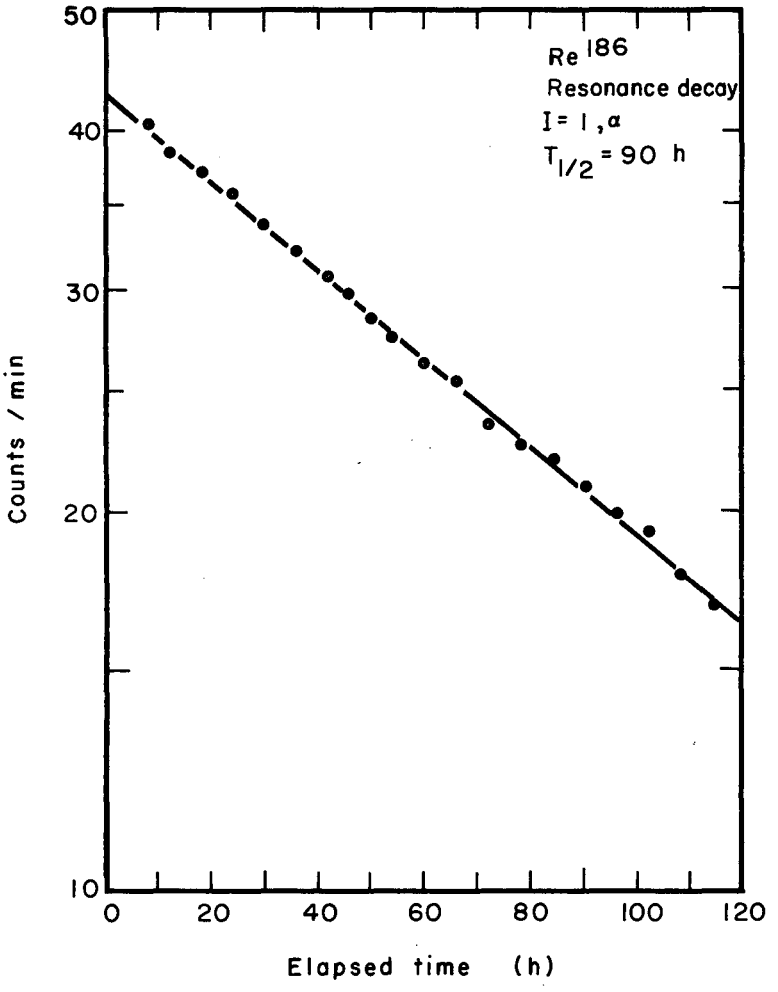

Fig. 24. Re^{186} resonance decay.

were traced out at 10.865 G and found to be centered at 21.520 Mc and 26.420 Mc, respectively, representing shifts of 340 kc and 180 kc from the Zeeman frequencies. The α transition is shown in Fig. 25.

E. Iridium

Iridium-192 ($T_{1/2}$ = 74 days) and iridium-194 ($T_{1/2}$ = 19 h) were produced by neutron bombardment of 0.010-in. wires. A flux of 5×10^{13} neutrons/cm^2/sec was sufficient, since the stable isotopes have very large capture cross sections. A 3-h bombardment produces about 0.5 Ci of activity with less than 10% Ir^{192}. This was all that we wished to handle, since Ir^{194} decays via the emission of high-energy β particles, and the radiation levels encountered were of the order of 100 roentgens at a distance of 1 ft from the sample. A 5-day bombardment produces 1.25 Ci of Ir^{192}, and a decay period of at least 7 days insures its predominance over the Ir^{194}.

The only observable levels in iridium are the ground level $d^7\text{-}^4F_{9/2}$ and the $d^8s\text{-}^4F_{9/2}$ level at 2835 cm^{-1}. These have $g_J = -1.30$ and $g_J = -1.33$, respectively, so that the resonances for the two levels are not resolved at low fields.

The energy-level diagram for Ir^{194} is given in Fig. 26 and the results are shown in Figs. 27 and 28. The second search yielded more information than the first, since it was made with a higher beam intensity. Again the notation is "I, F" and "exc" refers to the excited configuration. Resonances were observed for both $I = 1$ and $I = 4$. The beam contained about 10% Ir^{192}, as is shown by Fig. 29, but an ($I = 1$)-resonance exposure exhibited only 3% Ir^{192} (Fig. 30), indicating that $I = 1$ corresponds to the short-lived isotope. The relatively large intensity for $I = 4$ results because the ten transitions for this spin fall very close together. Runs made with a predominance of Ir^{192} (Figs. 31, 32, and 33) established the assignment $I = 4$ for this isotope, and the identity was confirmed by the decay curve, Fig. 34.

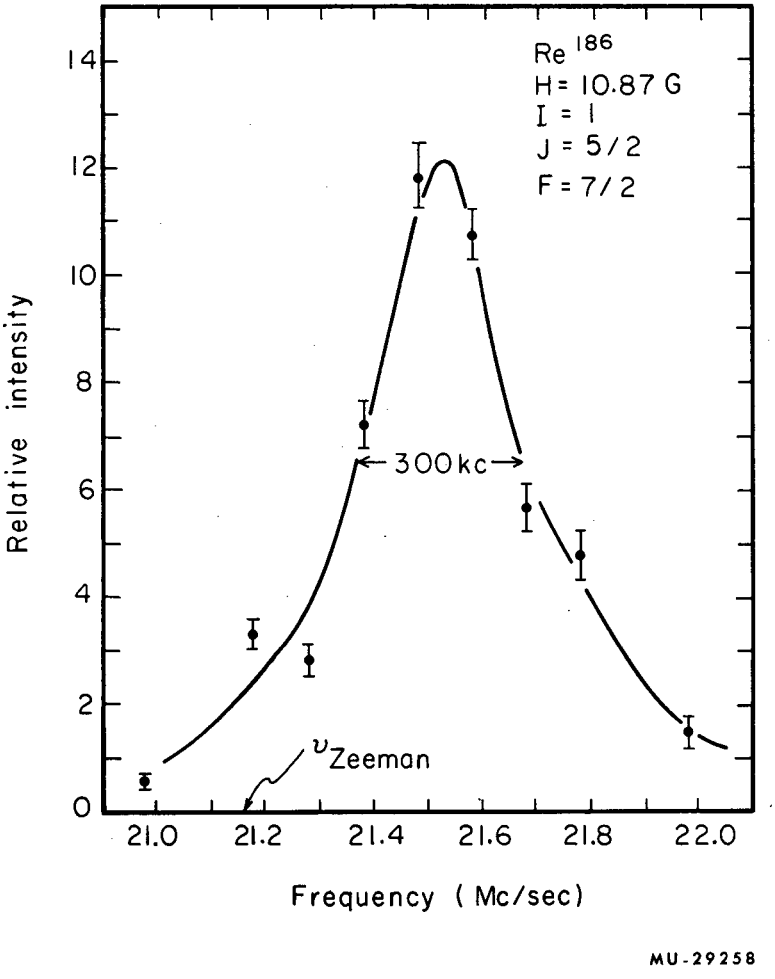

Fig. 25. Sample Re^{186} resonance.

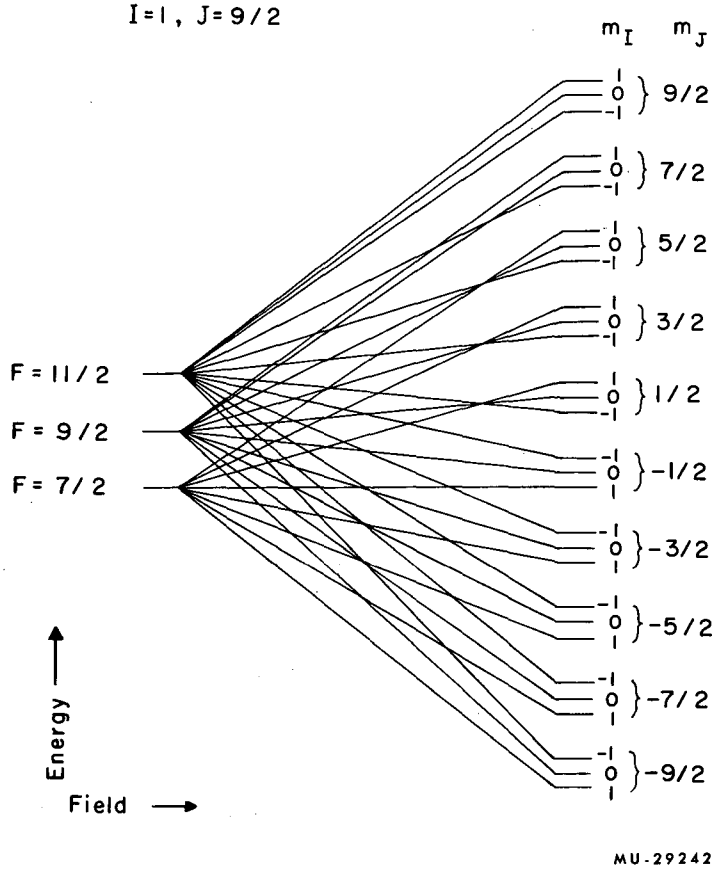

Fig. 26. Hfs levels of Ir^{194} (schematic).

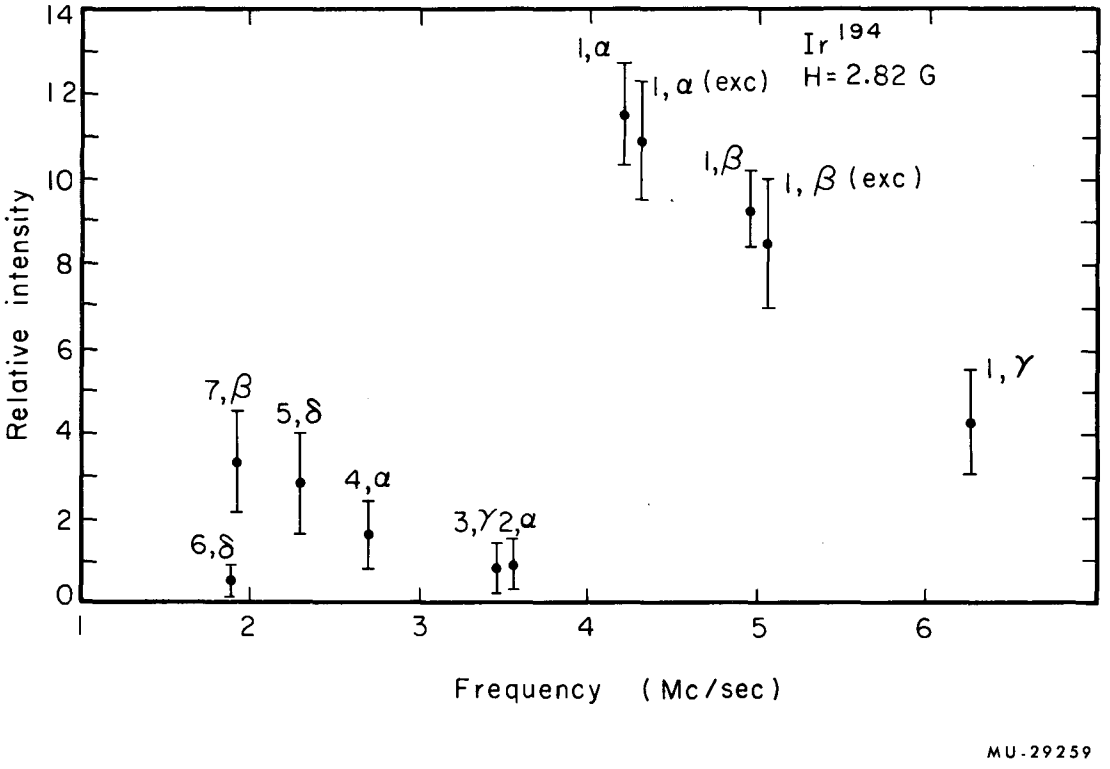

Fig. 27. Ir^{194} spin search.

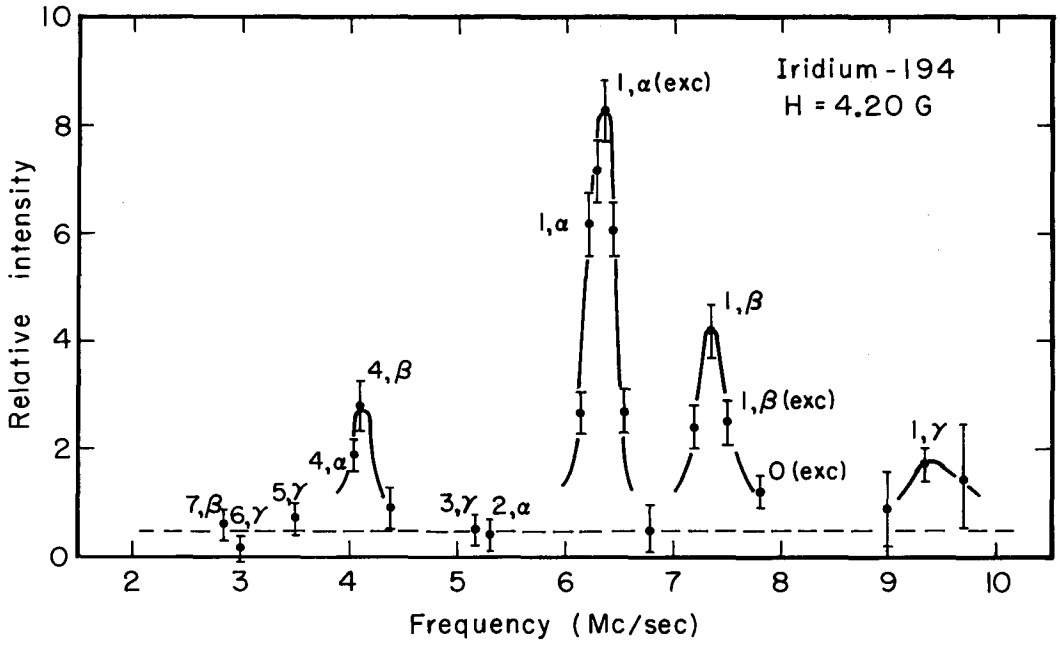

Fig. 28. Ir^{194} spin search.

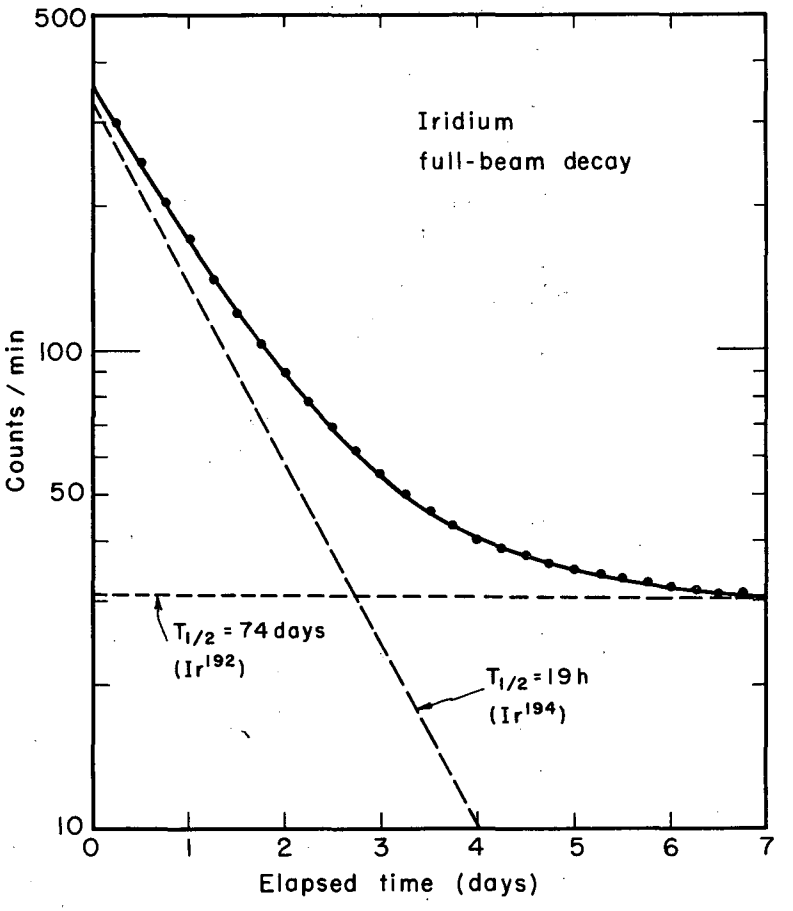

Fig. 29. Ir^{194} full-beam decay.

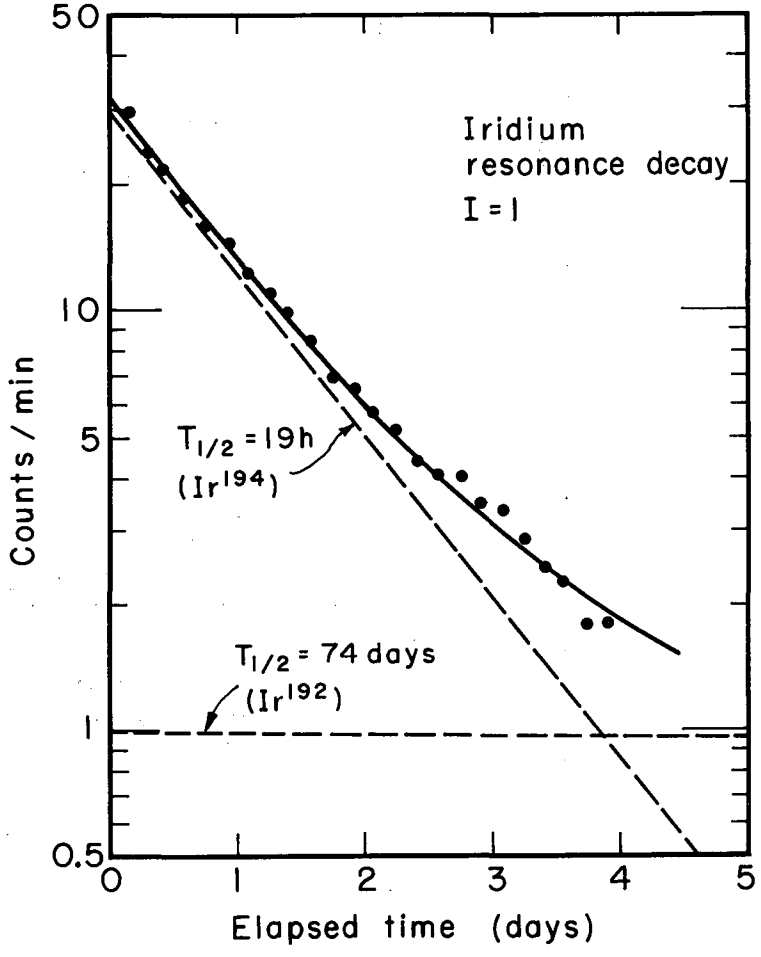

MU-28603

Fig. 30. Ir^{194} resonance decay.

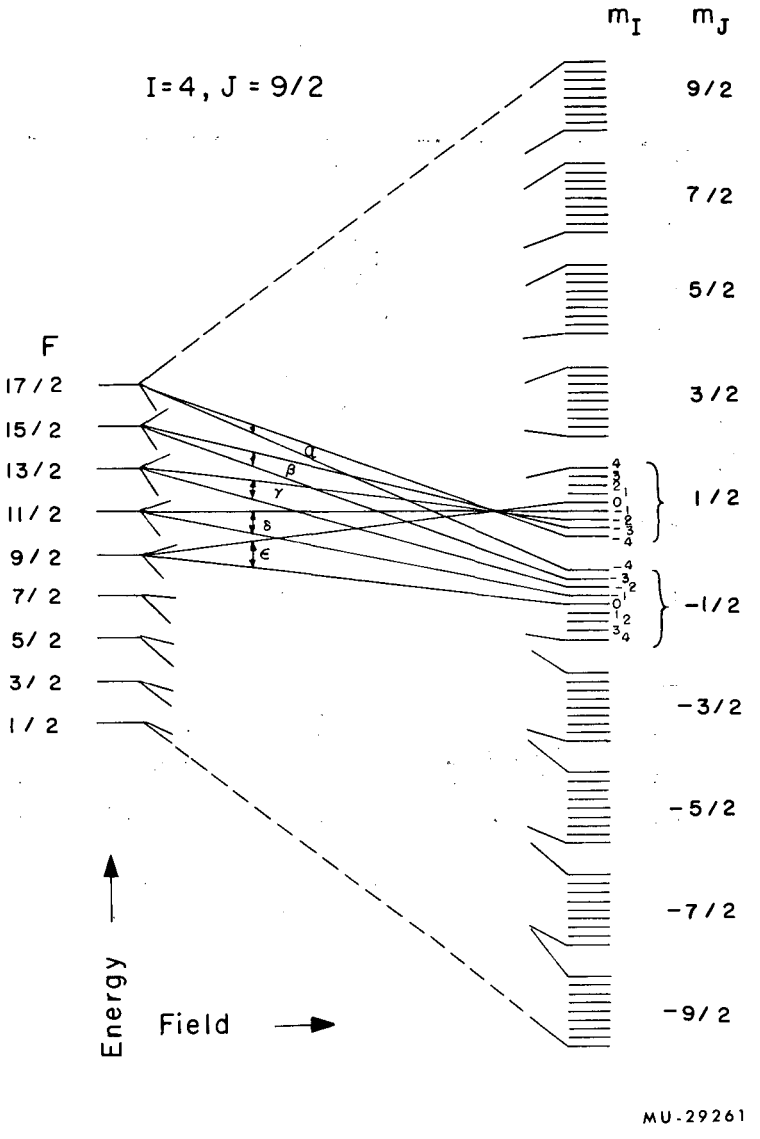

Fig. 31. Hfs levels of Ir^{192} (schematic).

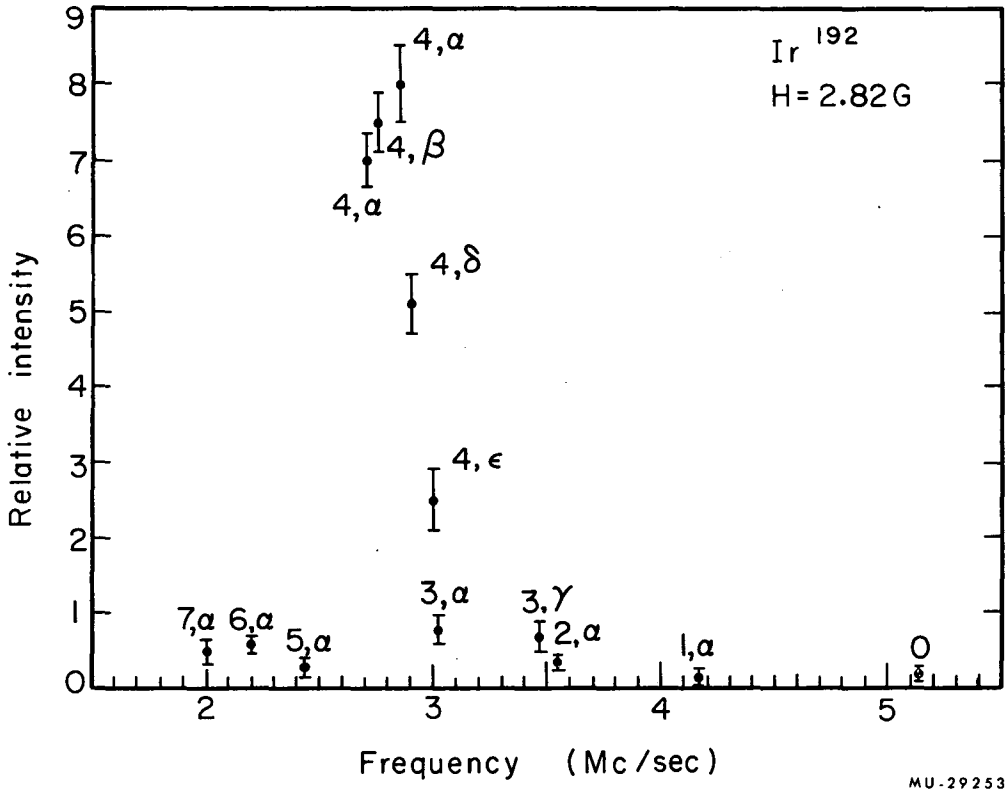

Fig. 32. Ir^{192} spin search.

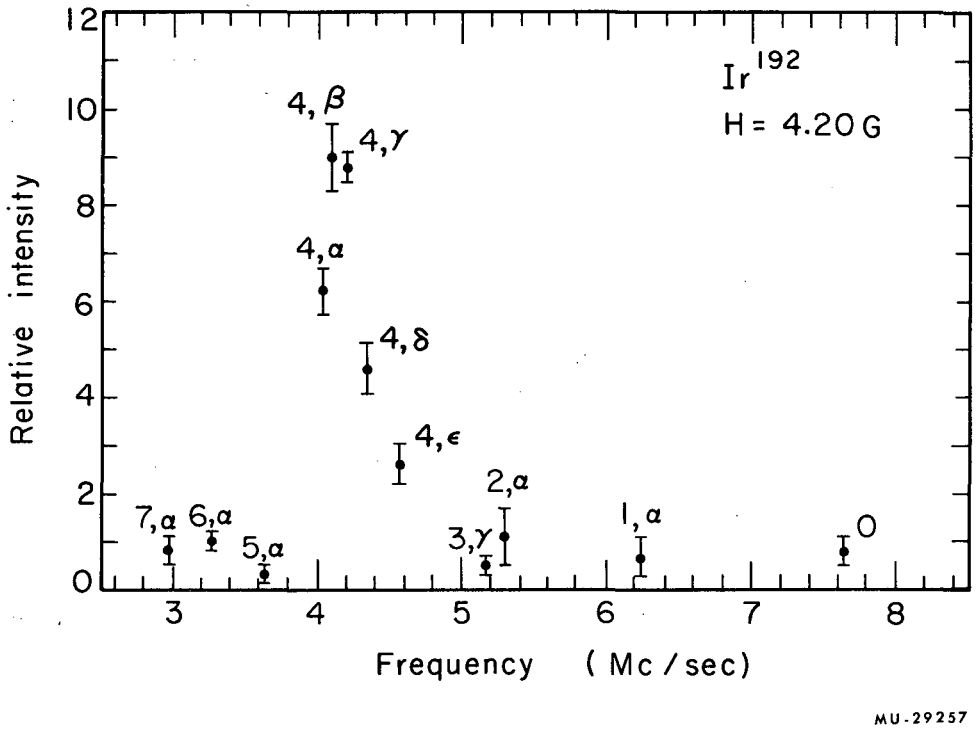

Fig. 33. Ir^{192} spin search.

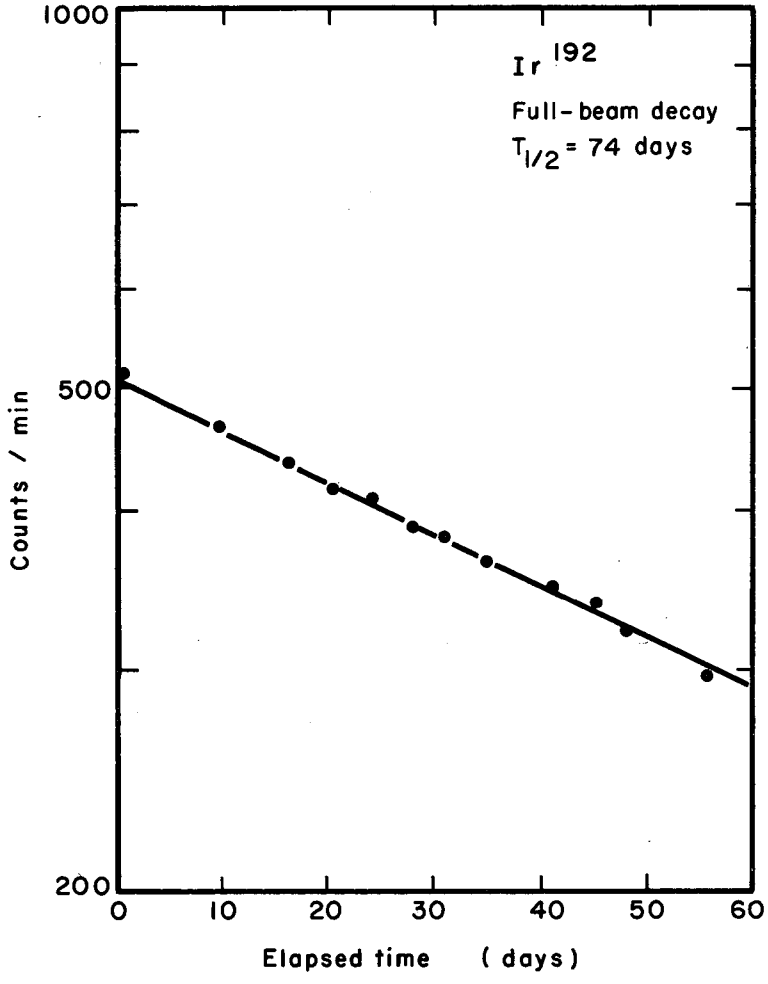

Fig. 34. Ir^{192} full-beam decay.

F. Tantalum

Tantalum 183 ($T_{1/2}$ = 5 days) was produced by a double-neutron-capture reaction in tantalum metal:

$$Ta^{181}(n, \gamma)Ta^{182}(n, \gamma)Ta^{183} .$$

The capture cross section of Ta^{182} is very large (about 20,000 b) so that a 10-day bombardment of a 0.020-in.-diam wire at 2×10^{14} neutrons/cm^2/sec yields about 10 Ci of activity of which less than 10% corresponds to Ta^{182}. The runs were made about 5 days after the sample had been removed from the reactor.

Our initial attempts to observe tantalum resonances were focused on the $^4F_{3/2}$ ground level of the configuration d^3. These proved unsuccessful. It was also observed that the throw-out (i.e., the ratio of the beam intensity obtained with the magnets off to that obtained with the magnets on) was very poor -- about 2:1 just below the melting point and even worse at lower temperatures. We concluded that the ground-state electronic g factor (g_J = -0.447) was too small to allow sufficient deflection of the tantalum beam, and thus decided to concentrate on the two observable excited states $^4F_{5/2}$ (g_J = -1.031) and $^4F_{7/2}$ (g_J = -1.218), and to increase the bombardment time and flux to the values given above. When the operating temperature was maintained just below the tantalum melting point, reproducible results were obtained which established the spin of Ta^{183} to be I = 7/2 (Figs. 35, 36, and 37). Full-beam and resonance decay plots are shown in Figs. 38 and 39.

Attempts were made to observe resonances in Ta^{182}, but we were unable to produce sufficient quantities of this isotope.

G. Interpretation

Measured nuclear spins in the region $150 < A < 190$ may be compared with those predicted by the unified model of the nucleus[39,34] in conjunction with the Nilsson individual-particle wave functions.[32] In

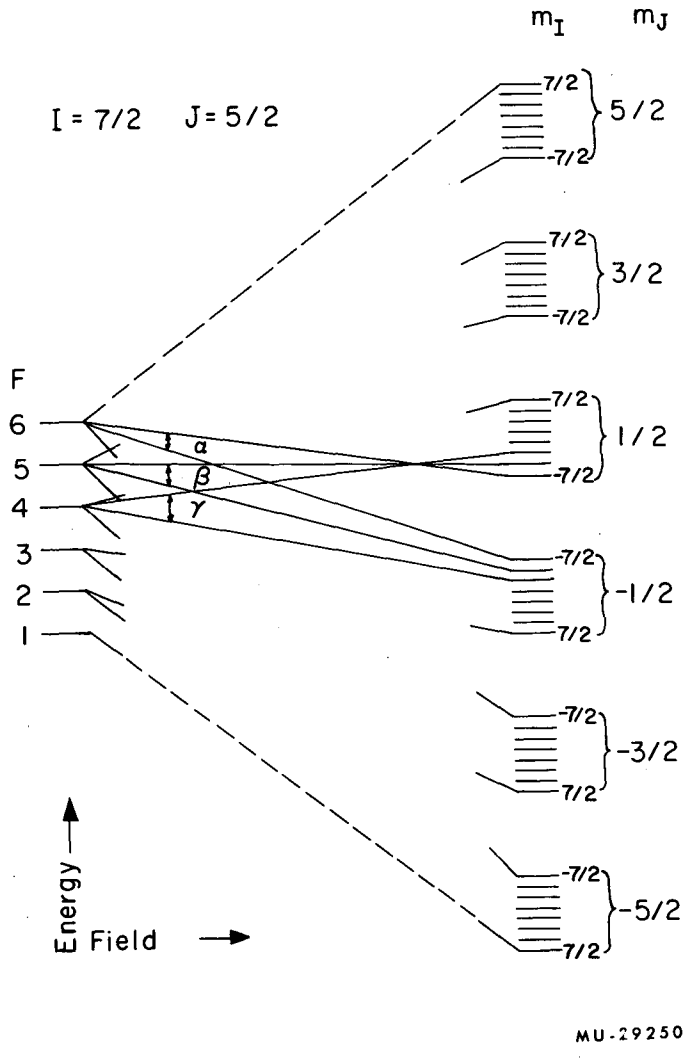

Fig. 35. Hfs levels of Ta^{183} (schematic).

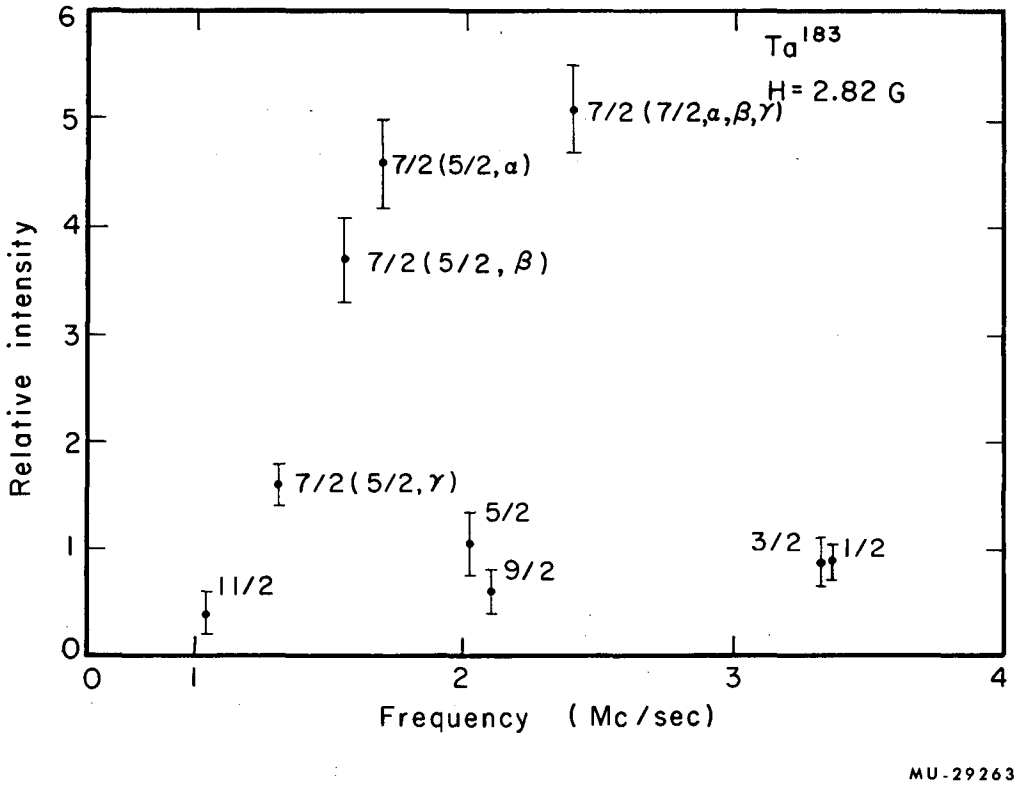

Fig. 36. Ta^{183} spin search.

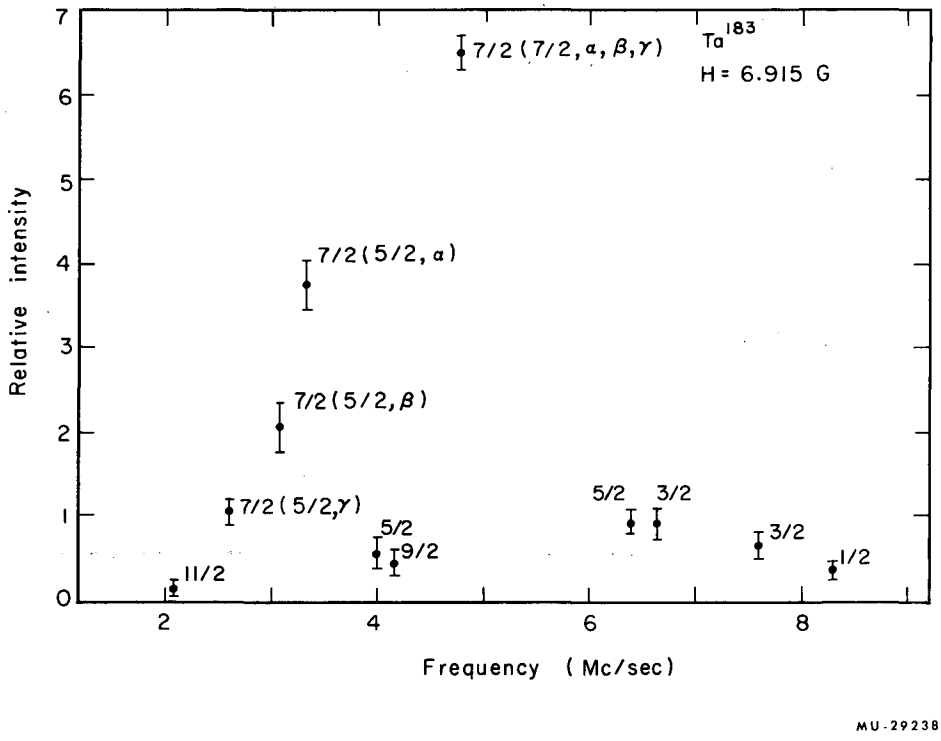

Fig. 37. Ta^{183} spin search.

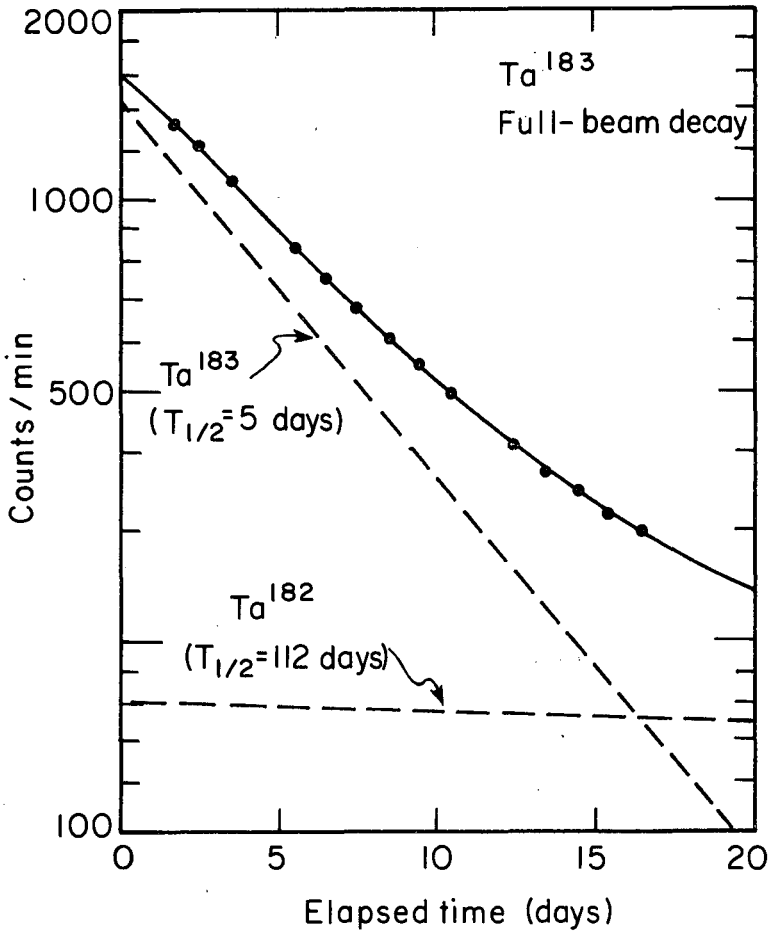

Fig. 38. Ta^{183} full-beam decay.

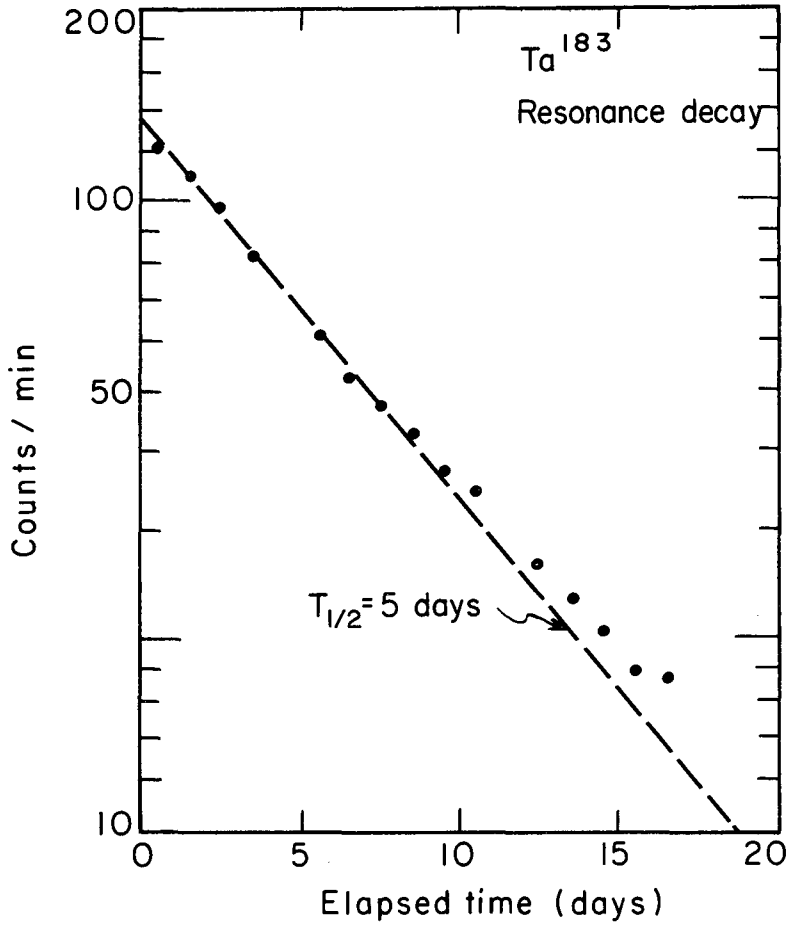

Fig. 39. Ta^{183} resonance decay.

the strong-coupling approximation, it is assumed that the nuclear equilibrium deformation, is sufficient to allow separation of those variables associated with the motion of the structure as a whole from those associated with the intrinsic motion of an individual particle. Such a separation is possible because the intrinsic particle motion will be relatively fast compared with the collective motion of the highly deformed structure. Nilsson's wave functions are based on the added assumptions that the particles move in an effective ellipsoidal deformation-dependent potential and that the collective structure is in the vibrational ground state.[32] The motion of an individual nucleon is characterized by the quantum number Ω_i representing the projection of its total angular momentum on the nuclear axis. The states are degenerate in $\pm\Omega_i$. With the exception of the case in which $\Omega = 1/2$, the nuclear spin in the rotational ground state is given by $I = \Omega$, where $\Omega = \sum_i \Omega_i$. Nucleons fill the available levels in pairs in the order of increasing energy so that, for an odd number of nucleons, the spin is equal to Ω_i for the unpaired particle. The Nilsson single-particle energy levels are shown in Figs. 40 and 41 as a function of deformation for protons in the region $50 < Z < 82$ and for neutrons in the region $82 < N < 126$. States are labeled by the extreme deformation quantum numbers $\Omega_i \alpha - [N\, n_z \Lambda_i]$, where N and n_z are the harmonic-oscillator quantum numbers, α is the parity, and Λ_i corresponds to the projection of the orbital angular momentum on the nuclear symmetry axis. Spins of strongly-deformed odd-odd nuclei are predicted by the coupling rules[40]

$$I = \Omega_p + \Omega_n \quad \text{if} \quad \Omega_p = \Lambda_p \pm 1/2 \quad \text{and} \quad \Omega_n = \Lambda_n \pm 1/2$$

and (36)

$$I = |\Omega_p - \Omega_n| \quad \text{if} \quad \Omega_p = \Lambda_p \pm 1/2 \quad \text{and} \quad \Omega_n = \Lambda_n \mp 1/2 \,.$$

All of the measured spins are compatible with these coupling rules after one makes the reasonable state assignments listed in Table V. The proton assignments are not in strict agreement with the level ordering of Fig. 40; however, added credibility is given to them

Table V. Individual particle states consistent with the measured nuclear spins.

Isotope	Measured spin (I)	Proton state	Neutron state	Assumed deformation (δ)
$^{110}_{73}Ta^{183}$	7/2	7/2-[404]	--	≈0.23
$^{111}_{74}W^{185}$	3/2	--	3/2-[512]	>0.22
$^{113}_{74}W^{187}$	3/2	--	3/2-[512]	0.19-0.22
$^{111}_{75}Re^{186}$	1	5/2-[402]	3/2-[412]	>0.22
$^{113}_{75}Re^{188}$	1	5/2-[402]	3/2-[512]	0.19-0.22
$^{115}_{77}Ir^{192}$	4	3/2-[402]	11/2-[615]	≈0.13
$^{117}_{77}Ir^{194}$	1	3/2-[402]	1/2-[510]	<0.07

because the stable isotopes of tantalum, rhenium, and iridium are known to have the spins $I = 7/2$ (Ta^{181}), $I = 5/2$ ($Re^{185/187}$), and $I = 3/2$ ($Ir^{191/193}$). It is worth noting that neither the level 9/2-[514] nor the level 11/2-[505], which compete with our assigned levels, has been observed as a nuclear ground state. This is perhaps due to a difference in the pairing energies associated with different levels.

The nuclear deformations shown in Table V are those for which the neutron-state assignments are consistent with Fig. 41. They are in agreement with deformations previously assigned in the region and with values calculated by Mottelson and Nilsson[33] (Fig. 42). As one would expect, there is a sudden decrease in deformation in the neighborhood of iridium. The agreement of the measured spins for this element with those predicted by the Nilsson model may in fact be partly fortuitous, since it is probable that there is a considerable mixing of intrinsic and collective modes of motion in the region, in which case the Nilsson states would not be expected to be a good approximation to the actual wave functions.

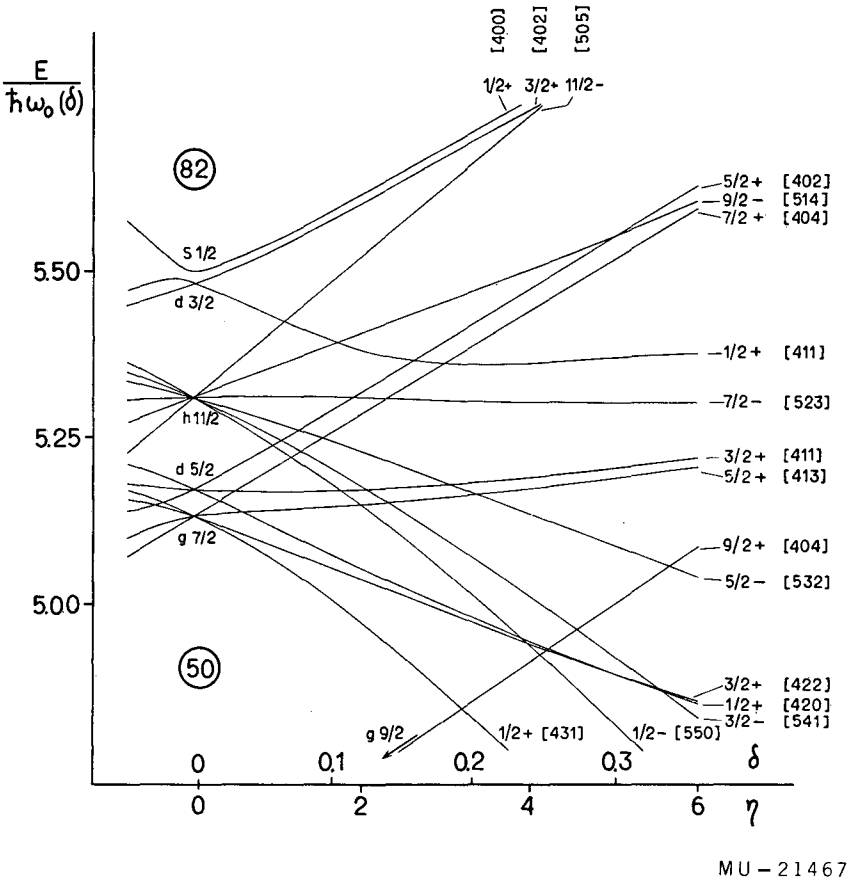

Fig. 40. Proton energy levels for $50 < Z < 82$ as a function of deformation, δ or η (after Mottelson and Nilsson).

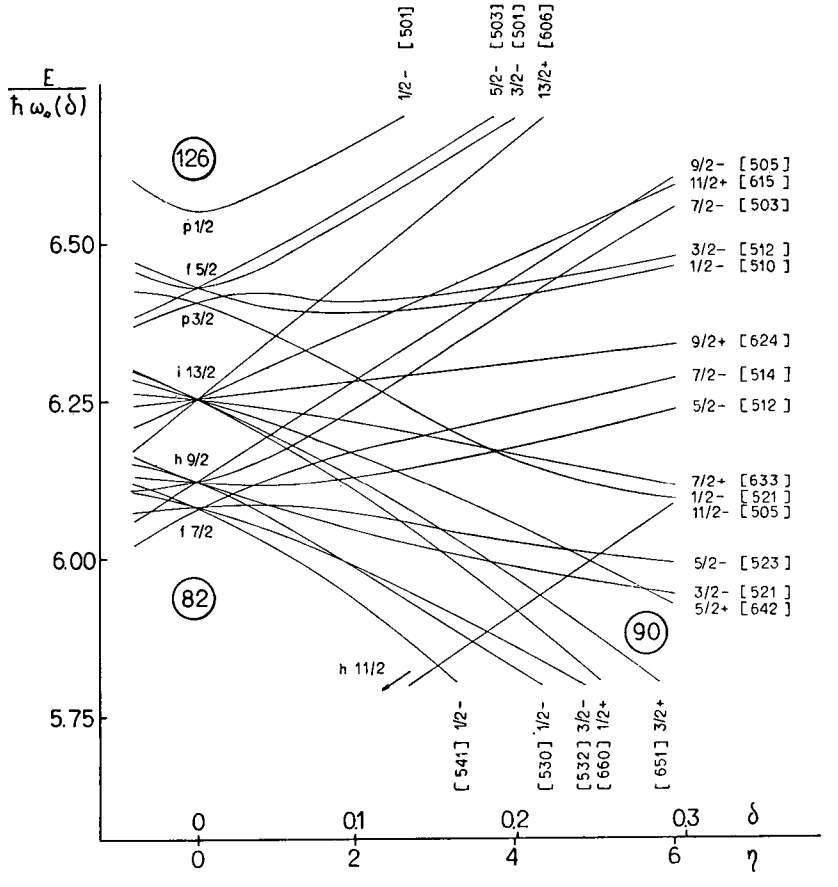

Fig. 41. Neutron energy levels for 82 < N < 126 (after Mottelson and Nilsson).

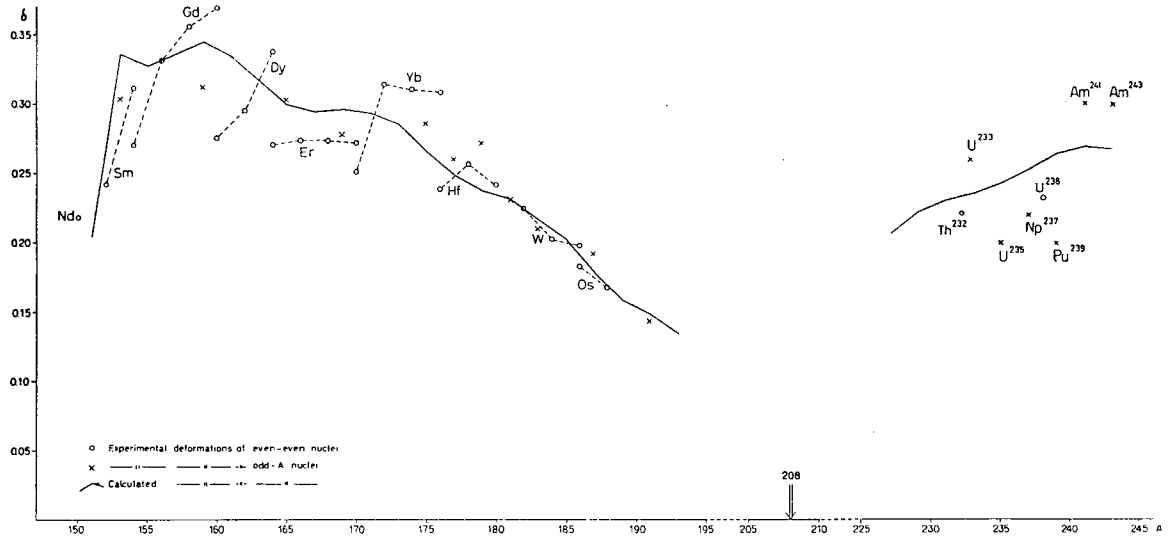

MU-28999

Fig. 42. Nuclear deformations. The solid line represents calculated values obtained by minimizing the total energy for a given configuration. The experimental values are obtained from observed E2 transition probabilities (after Mottelson and Nilsson).

ACKNOWLEDGMENTS

The completion of this work was made possible by the cooperation of many individuals. I would like especially to thank:

Professor William A. Nierenberg for his support;

Dr. Richard Marrus for his assistance and guidance in all aspects of the research;

Dr. Matthew White, Mr. Isaac Maleh, and Miss Dolores Ali for their counsel, assistance, and forbearance;

Mr. Douglas MacDonald for his engineering advice and aid;

My wife and my parents for their patience.

This work was performed under the auspices of the U. S. Atomic Energy Commission.

APPENDIX

Ground-State Wave Function For Erbium

The ground-state erbium wave function can be expressed as a linear combination of the two $J = 6$ Russell-Saunders eigenfunctions for the assumed configuration $(4f)^{12}$

$$|J = 6\rangle = \frac{1}{\sqrt{1+a^2}} |{}^3H_6\rangle + \frac{a}{\sqrt{1+a^2}} |{}^1I_6\rangle .$$

Determination of the constant a is equivalent to finding the unitary transformation that diagonalizes the $J = 6$ energy submatrix

$$\begin{pmatrix} E({}^3H_6) & \langle {}^3H_6 | \Lambda | {}^1I_6 \rangle \\ \langle {}^3H_6 | \Lambda | {}^1I_6 \rangle & E({}^1I_6) \end{pmatrix} .$$

The Coulomb energy has been given by Condon and Shortley in terms of the Slater radial integrals F_2, F_4, and F_6, and the spin-orbit energy may be expressed in terms of the parameter a_{4f}.[17] These quantities have been evaluated by Judd and Lindgren.[19] Thus, the required energies are

$$E({}^3H_6) = -25\, F_2 - 51\, F_4 - 13\, F_6 - 5/2\, a_{4f} = -18,594 \text{ cm}^{-1} ,$$

$$E({}^1I_6) = 25\, F_2 + 9\, F_4 + F_6 = 10,706 \text{ cm}^{-1} ,$$

and

$$\langle {}^3H_6 | \Lambda | {}^1I_6 \rangle = a_{4f} \langle -3^+ | \bar{\ell} \cdot \bar{s} | -2^- \rangle = 2735 \text{ cm}^{-1} .$$

Solution of the secular equation

$$\begin{vmatrix} E(^3H_6) - E'_{\pm} & \langle {}^3H_6 | \Lambda | {}^1I_6 \rangle \\ \langle {}^3H_6 | \Lambda | {}^1I_6 \rangle & E(^1I_6) - E'_{\pm} \end{vmatrix} = 0$$

yields the corrected energy levels for $J = 6$:

$$E'_{\pm} = \frac{1}{2}[E(^3H_6) + E(^1I_6)] \pm \frac{1}{2}\sqrt{[E(^3H_6)+E(^1I_6)]^2 - 4E(^3H_6)E(^1I_6) + 8\langle {}^3H_6 \Lambda {}^1I_6 \rangle^2}$$

and

$$E'_- = -20,600 \text{ cm}^{-1} .$$

The parameter a is now easily determined since

$$\mathcal{H}|J = 6\rangle = E'_-|J = 6\rangle ,$$

whence

$$\langle {}^1I_6 | \mathcal{H} | \psi \rangle = E'_- \langle {}^1I_6 | \psi \rangle .$$

Now,

$$\langle {}^1I_6 | \psi \rangle = \frac{a}{\sqrt{1+a^2}}$$

and

$$\langle {}^1I_6 | \mathcal{H} | \psi \rangle = \frac{1}{\sqrt{1+a^2}} [\langle {}^3H_6 | \Lambda | {}^1I_6 \rangle + a\, E(^1I_6)] ,$$

so that

$$a = \frac{\langle {}^3H_6 | \Lambda | {}^1I_6 \rangle}{[E'_- - E(^1I_6)]} = -0.087 .$$

REFERENCES

1. R. Marrus and W. A. Nierenberg, in Proceedings of the International School of Physics "Enrico Fermi" XVII Course (Academic Press, New York, 1962), p. 118.
2. C. Schwartz, Phys. Rev. 97, 380 (1955).
3. C. Schwartz, Phys. Rev. 105, 173 (1957).
4. N. F. Ramsey, Molecular Beams (Clarendon Press, Oxford, England, 1956).
5. I. I. Rabi, J. M. B. Kellogg, and J. R. Zacharias, Phys. Rev. 46, 157 (1934).
6. I. I. Rabi, J. R. Zacharias, S. Millman, and P. Kusch, Phys. Rev. 53, 318 (1938).
7. J. R. Zacharias, Phys. Rev. 61, 270 (1942).
8. H. Kopfermann, Nuclear Moments, E. E. Schneider, transl. (Academic Press, New York, 1958).
9. Gilbert O. Brink, Nuclear Spins of Thallium-197, Thallium-198m, Thallium-199, and Thallium-204 (Thesis), UCRL-3642, June 1957.
10. Joseph Winocur, Nuclear and Electronic Ground-State Properties of Pa^{233}, Am^{241}, and 16-h Am^{242} (Thesis), UCRL-9174, April 1960.
11. Seymour S. Alpert, The Moments, Spins, and Hyperfine Structures of the Radioactive Isotopes I^{133} (21h), Nd^{141} (2.5h), Eu^{152} (130 yr), and Bi^{210} (5 day) (Thesis), UCRL-9850, September 1961.
12. Matthew B. White, Hyperfine Structures and Nuclear Moments of Lu^{176m}, Br^{80}, Br^{80m}, and I^{132} (Thesis), UCRL-10321, September 1962.
13. A. Y. Gabezas, I. Lindgren, and R. Marrus, Phys. Rev. 122, 1796 (1961).
14. Donald H. Zurlinden (Lawrence Radiation Laboratory), private communication, 1962.
15. W. E. Lamb, Phys. Rev. 60, 817 (1941).
16. L. Landau and E. Lifshitz, The Classical Theory of Fields, Morton Hammermesh, Transl. (Addison-Wesley Publishing Co., Reading, Mass., 1951).

17. E. M. Condon and G. H. Shortley, Theory of Atomic Spectra (Cambridge University Press, 1935).
18. A. R. Edmonds, Angular Momentum in Quantum Mechanics (Princeton University Press, 1957).
19. B. R. Judd and I. Lindgren, Phys. Rev. 122, 1802 (1961).
20. R. Marrus, W. A. Nierenberg, and J. Winocur, Phys. Rev. 120, 1429 (1960).
21. H. Lew, Phys. Rev. 91, 619 (1953).
22. R. J. Elliott and B. W. H. Stevens, Proc. Roy. Soc. (London) A218, 553 (1953).
23. B. Bleaney, Proc. Phys. Soc. A68, 937 (1955).
24. E. C. Ridley, Proc. Cambridge Phil. Soc. 56, 41 (1960).
25. I. Lindgren, Nuclear Phys. 32, 151 (1962).
26. A. J. Freeman and R. E. Watson, Phys. Rev. 127, 2058 (1962).
27. D. Halford, Phys. Rev. 127, 1940 (1962).
28. G. J. Ritter, Phys. Rev. (to be published).
29. A. C. Gossard, V. Jaccarino, and J. H. Wernick, Bull. Am. Phys. Soc. 7, 482 (1962).
30. W. Low, Phys. Rev. 118, 1608 (1960).
31. A. H. Cooke and J. G. Park, Proc. Phys. Soc. (London) A69, 282 (1956).
32. S. G. Nilsson, Kgl. Danske Videnskab. Selskab, Mat.-Fys. Medd. 29, 16 (1955).
33. B. R. Mottelson and S. G. Nilsson, Kgl. Danske Videnskab. Selskab, Mat.-Fys. Skrifter, 1, 8 (1959).
34. A. Bohr and B. R. Mottelson, Kgl. Danske Videnskab. Selskab, Mat.-Fys. Medd. 27, 16 (1953).
35. R. J. Blin-Stoyle, Rev. Mod. Phys. 28, 75 (1956).
36. O. Kubaschewski and E. L. L. Evans, Mettallurgical Thermochemistry (Academic Press, New York, 1951).
37. C. E. Moore, Atomic Energy Levels (U. S. Government Printing Office, Washington, D. C., 1958).
38. V. S. Dubey, C. E. Mandeville, A. Mukerji, and V. R. Potnis, Phys. Rev. 106, 785 (1957).

39. A. Bohr, Phys. Rev. 81, 134 (1951).

40. C. J. Gallagher, Jr., and S. A. Moszkowski, Phys. Rev. 111, 1282 (1958).